11-4-2015

# Mesoporous Silica-Supported Amidozirconium-Catalyzed Carbonyl Hydroboration

Naresh Eedugurala
*Iowa State University*, eedug1n@iastate.edu

Zhuoran Wang
*Iowa State University*, zrwang@iastate.edu

Umesh Chaudhary
*Iowa State University*, umesse@iastate.edu

Nicholas C. Nelson
*Iowa State University*, nelsonnc@iastate.edu

Kapil Kandel
*Iowa State University*, kkandel@gmail.com

***See next page for additional authors***

# Mesoporous Silica-Supported Amidozirconium-Catalyzed Carbonyl Hydroboration

**Abstract**
The hydroboration of aldehydes and ketones using a silica-supported zirconium catalyst is reported. Reaction of Zr(NMe2)4 and mesoporous silica nanoparticles (MSN) provides the catalytic material Zr(NMe2)*n*@MSN. Exhaustive characterization of Zr(NMe2)*n*@MSN with solid-state (SS)NMR and infrared spectroscopy, as well as through reactivity studies, suggests its surface structure is primarily ≡SiOZr(NMe2)3. The presence of these nitrogen-containing zirconium sites is supported by 15N NMR spectroscopy, including natural abundance 15N NMR measurements using dynamic nuclear polarization (DNP) SSNMR. The Zr(NMe2)*n*@MSN material reacts with pinacolborane (HBpin) to provide Me2NBpin and the material ZrH/Bpin@MSN that is composed of interacting surface-bonded zirconium hydride and surface-bonded borane ≡SiOBpin moieties in an approximately 1:1 ratio, as well as zirconium sites coordinated by dimethylamine. The ZrH/Bpin@MSN is characterized by 1H/2H and 11B SSNMR and infrared spectroscopy and through its reactivity with D2. The zirconium hydride material or the zirconium amide precursor Zr(NMe2)*n*@MSN catalyzes the selective hydroboration of aldehydes and ketones with HBpin in the presence of functional groups that are often reduced under hydroboration conditions or are sensitive to metal hydrides, including olefins, alkynes, nitro groups, halides, and ethers. Remarkably, this catalytic material may be recycled without loss of activity at least eight times, and air-exposed materials are catalytically active. Thus, these supported zirconium centers are robust catalytic sites for carbonyl reduction and that surface-supported, catalytically reactive zirconium hydride may be generated from zirconium-amide or zirconium alkoxide sites.

**Keywords**
single-site catalysts, carbonyl hydroboration, zirconium hydride, interfacial catalysis, mesoporous silica, solid-state NMR

**Disciplines**
Chemistry

**Comments**
Reprinted (adapted) with permission from *ACS Catalysis* 5 (2015): 7399, doi: 10.1021/acscatal.5b01671.


**Authors**
Naresh Eedugurala, Zhuoran Wang, Umesh Chaudhary, Nicholas C. Nelson, Kapil Kandel, Takeshi Kobayashi, Igor I. Slowing, Marek Pruski, and Aaron D. Sadow

ACS Catalysis

Research Article

pubs.acs.org/acscatalysis

# Mesoporous Silica-Supported Amidozirconium-Catalyzed Carbonyl Hydroboration

Naresh Eedugurala, Zhuoran Wang, Umesh Chaudhary, Nicholas Nelson, Kapil Kandel,[‡] Takeshi Kobayashi, Igor I. Slowing, Marek Pruski,* and Aaron D. Sadow*

U.S. Department of Energy Ames Laboratory and Department of Chemistry, Iowa State University, 1605 Gilman Hall, Ames, Iowa 50011, United States

Supporting Information

**ABSTRACT:** The hydroboration of aldehydes and ketones using a silica-supported zirconium catalyst is reported. Reaction of $Zr(NMe_2)_4$ and mesoporous silica nanoparticles (MSN) provides the catalytic material $Zr(NMe_2)_n$@MSN. Exhaustive characterization of $Zr(NMe_2)_n$@MSN with solid-state (SS)NMR and infrared spectroscopy, as well as through reactivity studies, suggests its surface structure is primarily ≡SiOZr$(NMe_2)_3$. The presence of these nitrogen-containing zirconium sites is supported by $^{15}N$ NMR spectroscopy, including natural abundance $^{15}N$ NMR measurements using dynamic nuclear polarization (DNP) SSNMR. The Zr-$(NMe_2)_n$@MSN material reacts with pinacolborane (HBpin) to provide $Me_2$NBpin and the material ZrH/Bpin@MSN that is composed of interacting surface-bonded zirconium hydride and surface-bonded borane ≡SiOBpin moieties in an approximately 1:1 ratio, as well as zirconium sites coordinated by dimethylamine. The ZrH/Bpin@MSN is characterized by $^1H/^2H$ and $^{11}B$ SSNMR and infrared spectroscopy and through its reactivity with $D_2$. The zirconium hydride material or the zirconium amide precursor $Zr(NMe_2)_n$@MSN catalyzes the selective hydroboration of aldehydes and ketones with HBpin in the presence of functional groups that are often reduced under hydroboration conditions or are sensitive to metal hydrides, including olefins, alkynes, nitro groups, halides, and ethers. Remarkably, this catalytic material may be recycled without loss of activity at least eight times, and air-exposed materials are catalytically active. Thus, these supported zirconium centers are robust catalytic sites for carbonyl reduction and that surface-supported, catalytically reactive zirconium hydride may be generated from zirconium-amide or zirconium alkoxide sites.

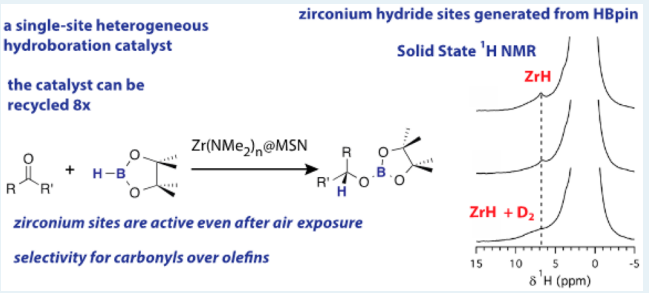


**KEYWORDS:** *single-site catalysts, carbonyl hydroboration, zirconium hydride, interfacial catalysis, mesoporous silica, solid-state NMR*

## INTRODUCTION

Surface-supported early-transition-metal hydrides[1,2] are highly reactive toward C−H bond breaking reactions that allow stoichiometric methane metalation[3] and catalytic conversions such as olefin polymerization,[4] hydrogenation,[5] H/D exchange,[6] alkane metathesis, and hydrogenolysis of polyethylene and other alkanes.[7−10] Although the surface provides kinetic stabilization of metal hydrides against multimetallic decomposition reactions, solution-phase early-metal and rare-earth hydrides are implicated in a range of catalytic chemistry including hydrosilylation,[11−17] hydrogenation,[18] dehydrocoupling and dehydrogenative polymerization,[19−21] and hydroboration.[22,23] Often, the metal hydrides in these reactions are generated and used in situ or are proposed as intermediates in catalytic cycles. This in situ generation could also be an advantageous approach for the application of surface-supported metal hydrides in catalysis. Moreover, a surface-supported hydride such as (≡SiO)$_3$ZrH could tolerate harsher conditions (e.g., higher temperature) than soluble analogues in catalytic addition chemistry, thereby permitting more difficult conversions as well as a straightforward means for recycling the catalytic materials.

We recently reported a homogeneous magnesium-catalyzed cleavage and hydroboration of esters using an in situ generated magnesium hydridoborate catalyst.[24] Despite the oxophilicity of the magnesium center, the catalytic site could be generated by reaction of pinacolborane (HBpin) and magnesium alkoxide. Similarly, [{Nacnac}MgH]$_2$ (Nacnac = ((2,6-*i*Pr$_2$C$_6$H$_3$)NCMe)$_2$HC) is a highly active catalyst for hydroboration of pyridines, ketones, and aldehydes.[22,25] A related zwitterionic magnesium catalyst is sufficiently reactive to reduce carbon dioxide to a methanol equivalent.[26] Hydroboration of aldehydes and ketones is catalyzed by soluble titanium,[27] molybdenum,[28] as well as a few late metal catalysts.[29,30] Recently, divalent germanium and tin compounds were also shown to catalyze this reaction, and hydrides were postulated intermediates.[31] Group 4-catalyzed carbonyl hydrosilylations and hydrogenations are

Received: July 31, 2015
Revised: October 29, 2015

  

DOI: 10.1021/acscatal.5b01671
*ACS Catal.* 2015, 5, 7399−7414

also known,[11,32−35] and although Schwartz's reagent catalyzes hydroboration of alkynes,[36] we are not aware of previous reports of zirconium-catalyzed hydroboration of carbonyls. In addition, the reaction of $Zr(NMe_2)_4$ and SBA-15 was recently reported to give an azazirconocyclopropane surface species,[37] as does a titanium amide on silica en route to a titanium imido.[38] Notably, the azazirconocyclopropane species reacts with hydrogen to give a zirconium hydride that catalyzes hydrogenation of olefins.[39] The catalytic C−H and C−C bond-breaking and -forming reactions of surface-supported zirconium hydride are notoriously sensitive to oxygen-containing impurities, which give irreversible deactivation of the catalytic sites.

As a possible solution to these deactivation processes, we envisioned that surface-supported oxophilic metal complexes with oxygen- or nitrogen-containing ligand precursors could be activated with reducing reagents such as boranes. Such transformations could potentially allow access to highly reactive surface-supported zirconium hydride sites under mild conditions and also provide a means for reactivating deactivated catalytic sites. On the basis of these ideas and the known chemistry of $(\equiv SiO)_3ZrH$,[1,3,40,41] the hydroboration of carbonyls appears to be an appropriate choice for testing the surface-supported Zr−OR bond cleavage steps in a catalytic cycle. Reductions of ketones and aldehydes are readily achieved with stoichiometric boron-containing reagents such as $BH_3$·THF or $NaBH_4$ or highly reactive metal hydrides such as $LiAlH_4$.[42,43] However, selectivity for carbonyls versus olefins and other functional groups including organohalides and nitro groups are limited with these reagents, these reagents are easily hydrolyzed by adventitious moisture, and their reactions produce substantial amounts of salt waste. Thus, alternative catalytic methods for selective carbonyl reductions, employing earth-abundant catalysts, are desirable. In this context, supported single-site hydroboration catalysts based on earth abundant zirconium would represent a significant conceptual advance in the field. In addition, a heterogeneous catalyst could offer advantages in sustainable synthesis through recyclable catalytic materials and in flow chemistry.

Here we report the synthesis and characterization of a mesoporous silica nanoparticle (MSN)-supported zirconium amide complex identified as $Zr(NMe_2)_n$@MSN. In the first section of this paper, we describe the details supporting the assigned surface structures of this material. In the second section, we describe the reactivity of $Zr(NMe_2)_n$@MSN with pinacolborane and the nature of the surface species ZrH/Bpin@MSN produced from that reaction. Finally, we present the catalytic activity of $Zr(NMe_2)_n$@MSN as a recyclable catalyst for the reduction of carbonyls by catalytic hydroboration.

## METHODS AND MATERIALS

**General.** All reactions were performed under a dry argon atmosphere using standard Schlenk techniques or under a nitrogen atmosphere in a glovebox, unless otherwise indicated. Dry, oxygen-free solvents were used throughout. Benzene, toluene, pentane, methylene chloride, and tetrahydrofuran were degassed by sparging with nitrogen, filtered through activated alumina columns, and stored under nitrogen. Benzene-$d_6$ was heated to reflux over Na/K alloy and vacuum-transferred. SBA-15 type MSN was synthesized according to the literature,[44] calcined at 550 °C, washed with water, and then heated to 550 °C under vacuum. The catalytic materials were characterized by $N_2$ sorption/desorption, powder XRD, TEM, solid-state $^1H$, $^2H$, $^{11}B$, $^{13}C$, and $^{15}N$ SSNMR spectroscopy, $^{15}N$ SSNMR spectroscopy enhanced by dynamic nuclear polarization (DNP), and infrared spectroscopy. $Zr(NMe_2)_4$,[45] $\{PhB(Ox^{Me2})_2C_5H_4\}Zr(NMe_2)_2$ ($Ox^{Me2}$ = 4,4-dimethyl-2-oxazoline),[46] $Si(SiMe_3)_4$,[47,48] and DBpin[49] were synthesized according to literature procedures. Pinacolborane (used as received) and 98% $^{15}N$-labeled $[H_2{}^{15}NMe_2]Cl$ (dried under vacuum at 120 °C for 2 h) were purchased from Aldrich. Solution-phase $^1H$, $^{13}C\{^1H\}$ and $^{11}B$ NMR spectra were collected either on a Bruker DRX 400 MHz spectrometer, Bruker Avance III 600 MHz spectrometer or a Varian MR 400 MHz spectrometer. $^{11}B$ NMR spectra were referenced to an external sample of $BF_3{\cdot}Et_2O$. Infrared spectra were recorded on neat MSN samples using a Bruker Vertex 80 spectrometer with a Harrick Praying Mantis Diffuse Reflection Accessory in a reaction chamber with ZnSe windows. These samples were prepared and maintained under an inert $N_2$ atmosphere. Elemental analyses were performed using a PerkinElmer 2400 Series II CHN/S in the Iowa State Chemical Instrumentation Facility.

Inductively coupled plasma-optical emission spectroscopy (ICP-OES) was performed on 10 samples to measure the zirconium loading in $Zr(NMe_2)_n$@MSN and zirconium and boron loading in ZrH/Bpin@MSN. The samples (2.0−4.0 mg each) were digested for 24 h in aqueous HF and HCl solution (0.18% and 5% respectively) and analyzed in a PerkinElmer Optima 2100 DV ICP-OES instrument.

$N_2$ sorption isotherms were measured in a Micromeritics Tristar surface area analyzer. Samples were previously purged for 6 h under a $N_2$ flow at 393 K, and the isotherms were determined at 77 K. The surface area was calculated using the Brunauer−Emmett−Teller equation, and the pore size distribution was obtained from analysis of the adsorption branch of the isotherm using the Barrett−Joyner−Halenda method.

Powder X-ray diffraction (XRD) patterns were obtained with a Rigaku Ultima IV diffractometer using a Cu target at 40 kV and 44 mA. K$\beta$ was removed with a monochromator, and the data were collected from 0.7 to 8 $2\theta°$ with a resolution of 0.02 $2\theta°$.

Transmission electron microscopy (TEM) and high-angle annular dark field scanning TEM (HAADF-STEM) images were acquired in a Tecnai G2 F20 electron microscope operated at 200 kV. Samples were prepared by dispersion into benzene, deposition of a single drop in a copper grid coated with lacey carbon, and evaporation at room temperature. Energy-dispersive X-ray (EDX) spectra were collected on representative areas to probe for homogeneity of elemental composition.

SSNMR measurements were performed on a 600 MHz Varian NMR System spectrometer, equipped with a 1.6 mm magic-angle spinning (MAS) probe. Several one-dimensional (1D) and two-dimensional (2D) experiments were used, including 1D $^1H$, $^2H$, $^{13}C$, and $^{11}B$ MAS with direct polarization (DPMAS), 1D $^1H \rightarrow {}^{13}C$ cross-polarization under MAS ($^{13}C$ CPMAS), $^{15}N$ CPMAS, $^{11}B$ CPMAS, 2D $^{11}B$ triple-quantum (3Q)MAS, as well as 2D $^1H-{}^{11}B$ heteronuclear correlation (Hetcor) NMR and indirectly detected $^{15}N-{}^1H$ (id)Hetcor NMR. The samples were packed in zirconia MAS rotors in a glovebox under nitrogen atmosphere. NMR experiments were carried out under $N_2$ atmosphere, as well.



DOI: 10.1021/acscatal.5b01671
ACS Catal. 2015, 5, 7399−7414

The $^{15}N$ DNP-enhanced CPMAS experiments were performed on a 400 MHz Bruker DNP SSNMR spectrometer equipped with a low-temperature (~100 K) MAS probe. The sample was prepared by impregnating the MSNs with a 16 mM solution of TEKPol in 1,1,2,2-tetrachloroethane (predried by stirring overnight with $CaCl_2$ followed by distillation under $N_2$), and then packed into a 3.2 mm sapphire MAS rotor.[50,51]

The SSNMR experimental parameters are given in the figure captions using the following symbols: $\nu_R$ denotes the MAS rate, $\nu_{RF}(X)$ is the magnitude of the RF field applied to X nuclei, $\tau_{CP}$ is the cross-polarization contact time, $\tau_{RD}$ is the recycle delay, and $\Delta t_1$ is the time interval of $t_1$ during 2D acquisition. $^1H/^{13}C$ and $^{15}N$ chemical shifts were referenced to TMS and nitromethane as 0 ppm, respectively.

**$Zr(NMe_2)_4$.** Labeled $H^{15}NMe_2$ was only available as $Me_2{}^{15}NH{\cdot}HCl$, so the synthesis of $Zr(NMe_2)_4$ from $Me_2NH{\cdot}HCl$ was developed, first with unlabeled starting material and then on small scale with the isotopically enriched material. Dried $Me_2NH{\cdot}HCl$ (0.500 g, 6.133 mmol) was suspended in tetrahydrofuran (50 mL) and cooled to −78 °C, and nBuLi (4.9 mL, 12.3 mmol) was added. The mixture was stirred at this temperature for 2 h and then warmed to room temperature and stirred for 12 h. The volatile components were evaporated under reduced pressure to give a solid residue, which was washed with pentane (3×) and dried under vacuum to yield a white solid mixture of $LiNMe_2$, LiCl and a substoichiometric amount of coordinated tetrahydrofuran. $^1H$ NMR (THF-$d_8$, 600 MHz): $\delta$ 3.63 (br, 1 H, THF), 2.70 (s, 6 H, $NMe_2$), 1.77 (br, 1 H, THF). $^{13}C\{^1H\}$ NMR (THF-$d_8$, 151 MHz): $\delta$ 68.3 (THF), 49.1 ($NMe_2$), 26.5 (THF). $^{15}N\{^1H\}$ NMR (THF-$d_8$, 59.2 MHz): $\delta$ −375.9.

The mixture of $LiNMe_2$ (0.370 g, 3.332 mmol of $LiNMe_2$) and LiCl was suspended in toluene. $ZrCl_4$ (0.110 g, 0.472 mmol) was added at room temperature, and the reaction mixture was stirred for 12 h. The solution was filtered, and the solvent was evaporated under reduced pressure to yield $Zr(NMe_2)_6Li_2THF_2$ (0.231 g, 0.449 mmol, 96%). $^1H$ NMR (benzene-$d_6$, 600 MHz): $\delta$ 3.35 (br, 8 H, THF), 3.19 (s, 36 H, $NMe_2$), 1.18 (br, 8 H, THF). $^{13}C\{^1H\}$ NMR (benzene-$d_6$, 151 MHz): $\delta$ 68.8 (THF), 46.9 ($NMe_2$), 25.7 (THF). $^{15}N\{^1H\}$ NMR (benzene-$d_6$, 59.2 MHz): $\delta$ −295.1.

$Zr(NMe_2)_6Li_2THF_2$ (0.200 g, 0.390 mmol) was dissolved in benzene. $ZrCl_4$ (0.045 g, 0.195 mmol) was added at room temperature, and the reaction mixture was stirred for 10 min. The solution was filtered, and the solvent was evaporated under vacuum to yield $Zr(NMe_2)_4$ (0.180 g, 0.673 mmol, 86%). The $^1H$ and $^{13}C\{^1H\}$ NMR spectra matched the reported literature values.[52] $^1H$ NMR (benzene-$d_6$, 600 MHz): $\delta$ 2.97 (s, $NMe_2$).

**$Zr(^{15}NMe_2)_4$.** The above procedure, employing $Me_2{}^{15}NH{\cdot}HCl$ (0.123 g, 1.12 mmol) and $ZrCl_4$ (0.036 g, 0.155 mmol), afforded $Zr(^{15}NMe_2)_6Li_2THF_2$ (0.074 g, 0.142 mmol, 93%). Reaction of this material with $ZrCl_4$ (0.033 g, 0.141 mmol) provided $Zr(^{15}NMe_2)_4$ (0.061 g, 0.225 mmol, 79%). $^1H$ NMR (benzene-$d_6$, 600 MHz): $\delta$ 2.98 (s, $NMe_2$). $^{15}N\{^1H\}$ NMR (benzene-$d_6$, 59.2 MHz): $\delta$ −306.2.

**$Zr(NMe_2)_n$@MSN.** A benzene solution of $Zr(NMe_2)_4$ (0.095 g, 0.355 mmol, 5 mL) was added to MSN (0.20 g, 0.34 mmol of SiOH groups) suspended in benzene (15 mL). The suspension was stirred for 20 h at ambient temperature, the mixture was centrifuged, and the solvent was decanted. The unreacted $Zr(NMe_2)_4$ was removed from the solid material by washing with benzene (3 × 5 mL) and then pentane (2 × 5 mL). The solid material was dried under vacuum yielding a white solid (0.253 g). IR (KBr, $cm^{-1}$): 2852 (m), 2777 (m), 1457 (m), 1084 (s, $\nu_{Si-O}$), 950 (m). Elemental analysis: Found: C, 5.91; H, 1.08; N, 3.44; Zr, 8.3 wt % (0.91 mmol).

**Bpin@MSN.** Pinacolborane (0.075 g, 0.594 mmol) dissolved in benzene was added to a suspension of calcined MSN (0.20 g, 0.34 mmol of SiOH) in benzene (5 mL). Vigorous bubbling was observed immediately. No more bubbling was observed after 2 h of stirring, the mixture was centrifuged, and the solvent was decanted. The unreacted HBpin was removed from the solid material by washing with benzene (3 × 5 mL) and then pentane (2 × 5 mL). The solid material was dried under reduced pressure yielding a white solid (0.226 g). IR (KBr, $cm^{-1}$): 2985 (m), 2938 (w), 1480 (m), 1456 (w), 1375 (m), 1223 (m), 1156 (m), 1086 (s, $\nu_{Si-O}$), 950 (m). Elemental analysis: Found: C, 9.99; H, 0.98; N, 0.03; B, 14.3 wt % (1.33 mmol).

**ZrH/Bpin@MSN.** Pinacolborane (0.691 g, 5.40 mmol) dissolved in benzene was added to $Zr(NMe_2)_n$@MSN (0.200 g, 0.182 mmol of Zr, 0.540 mmol of $NMe_2$) suspended in benzene (5 mL). Slow evolution of a small amount of bubbles was observed, and this bubbling was significantly reduced compared to the Bpin@MSN sample. The mixture was stirred at 60 °C for 2 h, allowed to settle in a centrifuge, and then the solvent was decanted. The unreacted HBpin and $Me_2NBpin$ were removed from the solid material by washing with benzene (3 × 5 mL) and pentane (2 × 5 mL). The solid material was dried under reduced pressure yielding a white solid (0.207 g). IR (KBr, $cm^{-1}$): 2979 (m), 2934 (w), 2805 (w), 1592 (w, Zr−H), 1479 (m), 1376 (w), 1095 (s, $\nu_{Si-O}$), 950 (m). Elemental analysis: Found: C, 8.09; H, 1.00; N, 0.51; Zr, 8.1 wt % (0.89 mmol); B, 9.3 wt % (0.86 mmol). Companion in situ micromolar scale reactions were performed in a J. Young-style Teflon-sealable NMR tube with 0.013 g $Zr(NMe_2)_n$@MSN, 0.041 g HBpin, and benzene-$d_6$ as solvent with a 7.48 mM $Si(SiMe_3)_4$ standard. From the integrated values of the $Me_2NBpin$ and $Si(SiMe_3)_4$ resonances, 0.102 mmol of $Me_2NBpin$ was formed.

**General Procedure for the Catalytic Hydroboration of Carbonyls (Aldehydes and Ketones) Using $Zr(NMe_2)_n$@MSN.** A mixture of the carbonyl substrate (1 mmol) and HBpin (1.3 mmol) was added to a $Zr(NMe_2)_n$@MSN (0.05 mmol Zr) that was suspended in benzene (10 mL). The reaction mixture was stirred for 10 h at room temperature for aldehydes or at 60 °C for ketones. The reaction mixture was filtered, the filtrate was quenched with 1 M aqueous NaOH solution, and the alcohol product was extracted with diethyl ether. The pure alcohol was obtained after drying the $Et_2O$ solution over $Na_2SO_4$ for 2 h and evaporating the solvent under reduced pressure.

## RESULTS AND DISCUSSION

**Synthesis and Characterization of $Zr(NMe_2)_n$@MSN.** Tetrakis(dimethylamido)zirconium was grafted on high surface area mesoporous silica to give $Zr(NMe_2)_n$@MSN. The silica support, in the form of SBA-15 type MSN characterized by a hexagonal array (*p6mm*) of 9.7 nm diameter pores and a surface area of 385 $m^2/g$, was produced by hydrolysis−condensation of tetramethylorthosilicate using the Pluronic P104 template, calcined at 550 °C, washed with water, then heated at 550 °C under vacuum, and subsequently stored in a glovebox away from ambient air and moisture.[44] The SiOH group surface concentration of 1.7 mmol/g was determined by measuring the concentration of toluene produced in a titration with



DOI: 10.1021/acscatal.5b01671
ACS Catal. 2015, 5, 7399−7414

$Mg(CH_2Ph)_2(O_2C_4H_8)_2$[53] and by spin counting of $Q^3$-sites with $^{29}Si$ DPMAS NMR spectroscopy (1.6 mmol/g). Thus-prepared MSN and $Zr(NMe_2)_4$ react in benzene at room temperature for 20 h producing $Zr(NMe_2)_n$@MSN, a grafted material that we will contend is primarily monopodal tris(dimethylamido)zirconium, with smaller amounts of bipodal species bis(dimethylamido)zirconium and bis(dimethylamido)(dimethylamino)zirconium (eq 1).

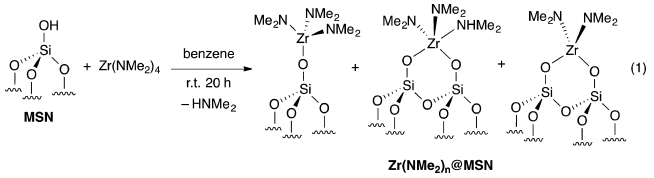


Upon scale-up, the $Zr(NMe_2)_n$@MSN is purified from excess $Zr(NMe_2)_4$ by pentane and benzene washes. The structural morphology of the material was characterized by powder XRD and TEM. The zirconium sites were identified and characterized by the mass-balance implied by stoichiometry from the synthesis, quantitative metals analysis using ICP-OES, combustion analysis, infrared spectroscopy, and SSNMR spectroscopy, as well as the stoichiometry and observed products of its reactions with HBpin and $D_2$.

A TEM image (Figure 1A) of $Zr(NMe_2)_n$@MSN showed that the ordered mesoporous nature of the SBA-15-type material is maintained after its treatment with $Zr(NMe_2)_4$. There was no evidence for large zirconium clusters formed in the grafting experiments in the images produced by TEM and HAADF-STEM (Figure 1B). Likewise, the EDX analysis (Figure 1C) suggested that zirconium is well dispersed over the silica. In addition, a powder XRD measurement of $Zr(NMe_2)_n$@MSN showed diffraction peaks assigned to the periodic channels of the mesoporous silica support (see Supporting Information (SI) Figure S1).

Next, the amount of $Zr(NMe_2)_4$ grafted onto MSN was approximated by quantifying the soluble zirconium amide before and after its reaction with the silica. A benzene solution of excess $Zr(NMe_2)_4$ (1.78 mmol) stirred with 1 g of MSN resulted in the consumption of 1 mmol of $Zr(NMe_2)_4$, indicating that the loading is ca. 1 mmol Zr per gram of MSN. In this reaction, approximately 1.2 mmol of $HNMe_2$ was produced per gram of silica. These amounts were determined by integration of the reactant and product resonances in $^1H$ NMR spectra of the reaction mixtures, which contained a known concentration of $Si(SiMe_3)_4$ as an internal standard. This loading was further supported by ICP-OES analysis that indicated the presence of 8.4 ± 0.1 wt % Zr in $Zr(NMe_2)_n$@MSN (0.91 ± 0.1 mmol Zr/g; Table 1). The ICP-OES analysis involved 10 measurements performed over several days on samples of $Zr(NMe_2)_n$@MSN and established the stability of the zirconium-supported material and the reproducibility of the method for the comparison of the series of materials derived from $Zr(NMe_2)_n$@MSN. Heating of $Zr(NMe_2)_n$@MSN at 60 °C in benzene did not affect the material's weight %.

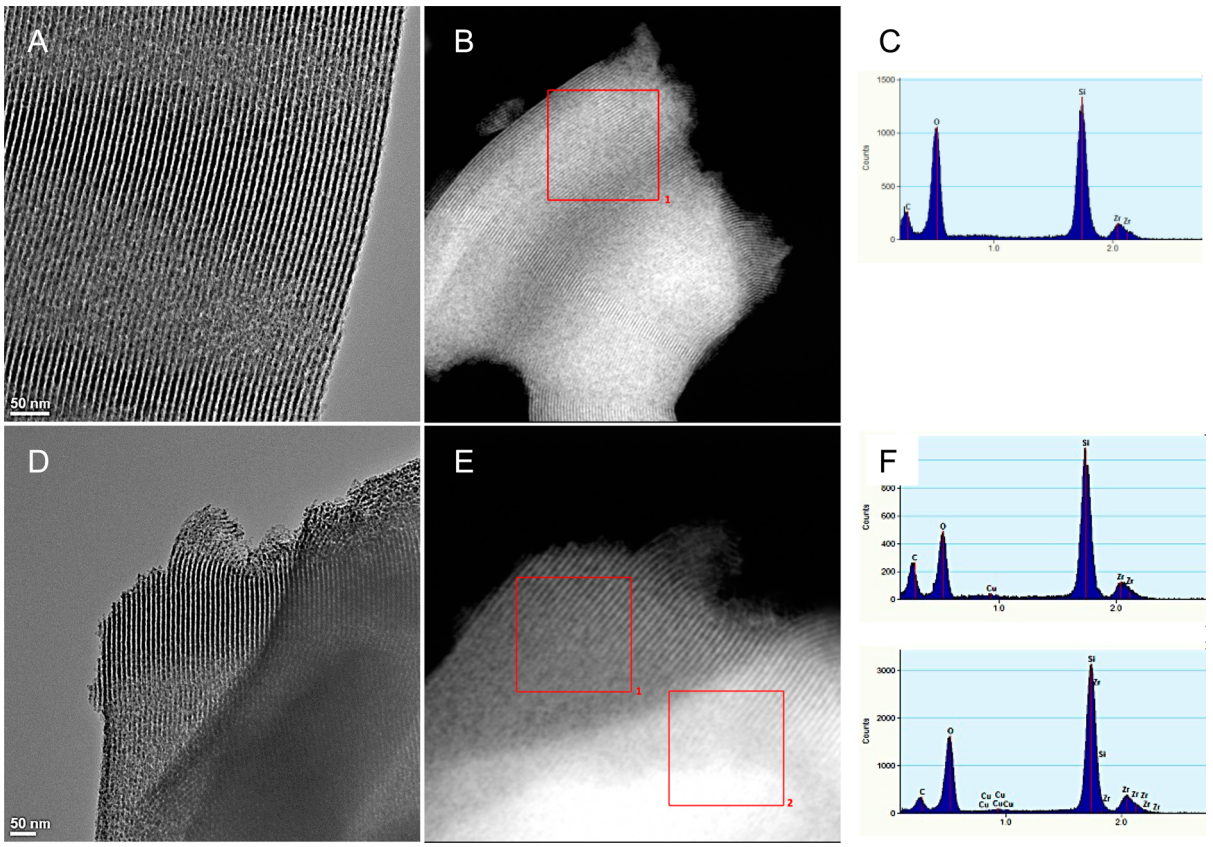


**Figure 1.** (A) TEM of $Zr(NMe_2)_n$@MSN, (B) HAADF-STEM of $Zr(NMe_2)_n$@MSN, (C) EDX analysis of the region enclosed in the red square in the HAADF-STEM image of $Zr(NMe_2)_n$@MSN, (D) TEM of $Zr(NMe_2)_n$@MSN + HBpin, (E) HAADF-STEM of $Zr(NMe_2)_n$@MSN + HBpin, and (F) EDX analysis of the regions enclosed in the red squares in the HAADF-STEM image showing consistent Zr:Si ratios throughout the material.



DOI: 10.1021/acscatal.5b01671
ACS Catal. 2015, 5, 7399–7414

Table 1. Zirconium Loading of $Zr(NMe_2)_n$@MSN Materials Obtained by ICP-OES Analysis

| material preparation | conditions[a] | weight % Zr[b] | mmol Zr/g |
|---|---|---|---|
| $Zr(NMe_2)_4$ + MSN → $Zr(NMe_2)_n$@MSN | 20 h, r.t. | 8.4 ± 0.1 | 0.91 |
| $Zr(NMe_2)_n$@MSN heated at 60 °C | 2 h, 60 °C | 8.4 ± 0.1 | 0.92 |
| $Zr(NMe_2)_n$@MSN + 10 HBpin → ZrH/Bpin@MSN | 2 h, 60 °C | 8.2 ± 0.1 | 0.89 |
| $Zr(NMe_2)_n$@MSN + 10 HBpin +10 PhMeC=O | 2 h, 60 °C | 8.2 ± 0.1 | 0.89 |

[a]Benzene solvent. [b]Determined by ICP-OES analysis.

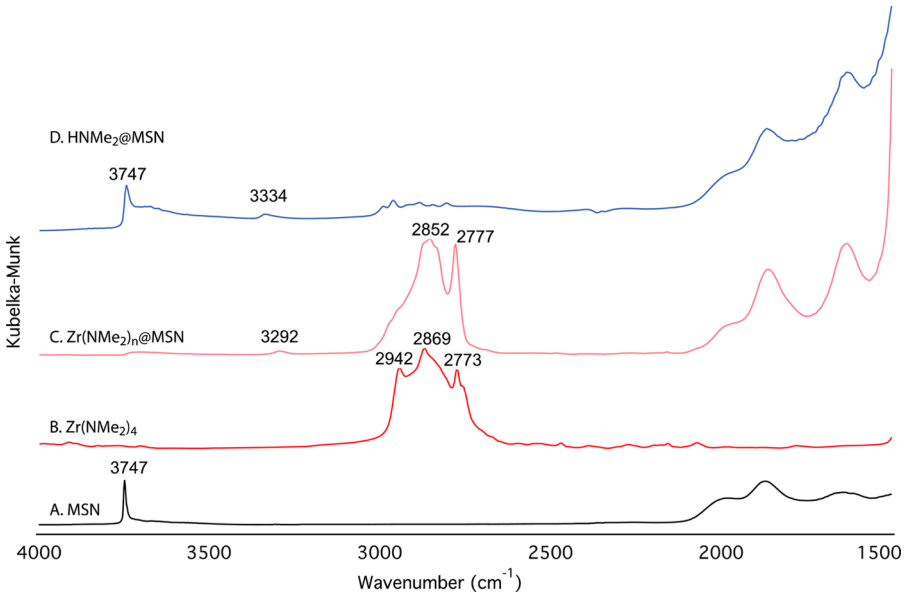


**Figure 2.** Diffuse reflectance infrared spectra of (A) MSN, (B) $Zr(NMe_2)_4$, (C) $Zr(NMe_2)_n$@MSN, and (D) MSN + $HNMe_2$.

The Zr:$NMe_2$ ratio in $Zr(NMe_2)_n$@MSN, as well as the carbon (5.91%, 4.9 mmol/g), hydrogen (1.08%, 10.8 mmol/g), and nitrogen (3.44%, 2.5 mmol/g) loadings were measured using combustion analysis. From these data, the Zr:C:N ratio is 1:5.4:2.7 corresponding to a Zr:$NMe_2$ ratio of 1:2.7. These results, corroborated by the measurements of the stoichiometry of the grafting reactions, imply that the material contains primarily zirconium sites with three nitrogen-containing ligands and a smaller amount (up to 30%) of sites with two nitrogen-containing ligands.

The presence of $NMe_2$ groups in $Zr(NMe_2)_n$@MSN was identified through infrared spectroscopy. An IR spectrum of MSN (calcined, washed with water, and then dried at 550 °C under vacuum) contained an absorption at 3747 $cm^{-1}$ assigned to isolated SiOH groups (Figure 2A).[54] Also, for comparison, the infrared spectrum of $Zr(NMe_2)_4$ contained bands at 2942, 2869, 2773, and 1457 $cm^{-1}$ (Figure 2B; see Figures S2 and S3 for full IR spectra).

After the reaction between MSN and $Zr(NMe_2)_4$, several new signals associated with organic groups were observed at 2852, 2777, and 1457 $cm^{-1}$. These signals are similar to those observed for $Zr(NMe_2)_4$, as can be seen through comparison of Figure 2B,C. After the grafting reaction, the IR band associated with isolated surface SiOH moieties was diminished, and it is likely that some unreacted SiOH groups are still present on the surface. These groups, as well as likely NH containing species, are difficult to detect as a result of their low concentration and possible broadening due to hydrogen bonding.

The $HNMe_2$ reaction byproduct might be expected to interact with the silica surface. To test for this possibility, MSN and $HNMe_2$ were allowed to react in benzene, pentane, or under solid−gas conditions (Figure 2D) in three independent experiments, followed by evacuation. In all cases, a small signal at 1457 $cm^{-1}$ and even weaker intensity signals typically attributed to $\nu_{CH}$ or $\nu_{NH}$ (at 3334 $cm^{-1}$) were observed in the infrared spectra. The peak at 3747 $cm^{-1}$ assigned to isolated SiOH groups was observed after the $HNMe_2$ treatments. In addition, a weak, yet sharp signal was observed in the $^{13}C$ CPMAS spectrum (not shown), with the chemical shift very close to neat dimethylamine (~35 ppm) and the intensity corresponding to less than 0.1 mmol/g. From these experiments, we conclude that only a small amount of $HNMe_2$ associates with the MSN material in physisorbed form. Moreover, these sites may be blocked once zirconium amide is grafted to the silica surface.

The $^{13}C$ CPMAS SSNMR spectrum of $Zr(NMe_2)_n$@MSN (Figure 3, top) showed two strongly overlapping signals with the chemical shifts of ~36 and ~39 ppm, which are similar to that of $Zr(NMe_2)_4$ dissolved in benzene-$d_6$ (42 ppm). No other resonances were detected, even after 76 000 acquisitions. The completeness of the CPMAS spectrum was confirmed by the $^{13}C$ DPMAS experiment (Figure 3, bottom), which yielded the same line shape. These $^{13}C$ spectra contrast with those reported earlier by El Eter et al., in which $\equiv SiOZr(\eta^2\text{-}CH_2NMe)(NMe_2)(NHMe_2)$, formed from the reaction of $SBA\text{-}15_{700}$ (i.e., mesoporous silica pretreated at 700 °C) and $Zr(NMe_2)_4$ in pentane for 1 h produced three signals at 36, 47, and 85 ppm.[37]

DFT calculations showed that the chemical shifts of all methyl carbons in dimethylamido zirconium model surface moieties, including $\equiv SiOZr(NMe_2)_3$ and $(\equiv SiO)_2Zr(NMe_2)_2$, are expected between 36 and 43 ppm (see Figure S4 in SI), strongly supporting the hypothesis that both



DOI: 10.1021/acscatal.5b01671
ACS Catal. 2015, 5, 7399−7414

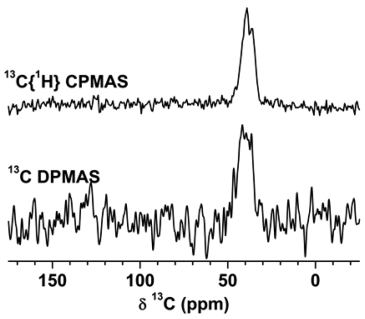


**Figure 3.** $^{13}$C CPMAS (top) and DPMAS (bottom) spectra of $Zr(NMe_2)_n$@MSN obtained under 25 kHz MAS with $^{1}$H TPPM heteronuclear decoupling at $\nu_{RF}(^{1}H)$ = 100 kHz. The CPMAS spectrum was measured using $\nu_{RF}(^{1}H)$ = 75 kHz and $\nu_{RF}(^{13}C)$ = 100 kHz during CP, $\tau_{CP}$ = 4.5 ms, $\tau_{RD}$ = 1.5 s, and 76 000 scans. The DPMAS spectrum resulted from 360 scans with $\tau_{RD}$ = 60 s.

resonances observed in $Zr(NMe_2)_n$@MSN represent the Zr-bound $NMe_2$ functionalities. As detailed in the SI, the DFT calculations were based on the gauge-including projector-augmented wave (GIPAW) method.[55] The observed non-equivalence of methyl groups can be attributed to differences in local geometries and mobilities (see eq 1).

Spin counting, using a $^{13}$C DPMAS NMR experiment, quantified the $NMe_2$ loading in $Zr(NMe_2)_n$@MSN at 2.7 (±0.5) mmol/g. Considering the fact that the Zr loading measured with ICP-OES was 0.91 mmol/g, the Zr:$NMe_2$ ratio is estimated at close to 1:3. This value and the value obtained from combustion analysis (1:2.7) described above are in sufficient agreement to suggest the surface species in $Zr(NMe_2)_n$@MSN primarily comprises three nitrogen-containing ligands, although some quantity of bipodal $(\equiv SiO)_2Zr(NMe_2)_2$ (up to 30%) is likely to be present. The former species may be either the monopodal $\equiv SiOZr(NMe_2)_3$ or a dipodal diamido amine adduct $(\equiv SiO)_2Zr(NMe_2)_2(NHMe_2)$. The monopodal stoichiometry would imply that ∼0.7−0.8 mmol/g of ≡SiOH remained intact, and indeed, the experiments with pinacolborane described below suggest that accessible ≡SiOH groups remain on the silica surface. In contrast, the diffuse reflectance FTIR spectrum does not contain signals in the expected region for isolated SiOH. That is, neither the IR peak at 3747 $cm^{-1}$, associated with isolated silanols, nor a broad signal for hydrogen-bonded silanols are observed. However, a weak signal at 3292 $cm^{-1}$ may be assigned to an NH stretching band of a possible zirconium-coordinated dimethylamine, and this signal is slightly shifted from the signal of physisorbed $HNMe_2$ on MSN. On the basis of the residual nitrogen loading after treatment of $Zr(NMe_2)_n$@MSN with HBpin (see below), the amount of zirconium-coordinated dimethylamine is estimated to be less than 10%.

Because $\equiv SiOZr(NMe_2)_3$, $(\equiv SiO)_2Zr(NMe_2)_2(NHMe_2)$, or $(\equiv SiO)_2Zr(NMe_2)_2$ are not conclusively distinguished as surface structures by $^{13}$C SSNMR, IR, and elemental analysis, we turned to $^{15}$N SSNMR measurements to further characterize the nitrogen-containing ligands bonded to zirconium. At natural $^{15}$N abundance, NMR signals could not be detected either in 1D $^{15}$N spectra or in 2D $^{1}$H−$^{15}$N correlation experiments. We thus resorted to the newly developed DNP method, which enhances the sensitivity of SSNMR of surface species by ∼2 orders magnitude via excitation of the exogenously introduced biradicals (here TEKPol dissolved in 1,1,2,2-tetrachloroethane) at their ESR resonance frequency, followed by transfer of magnetization to the nuclear spins.[50,51] A high-quality DNP-enhanced $^{15}$N CPMAS spectrum of $Zr(NMe_2)_n$@MSN was indeed acquired under natural

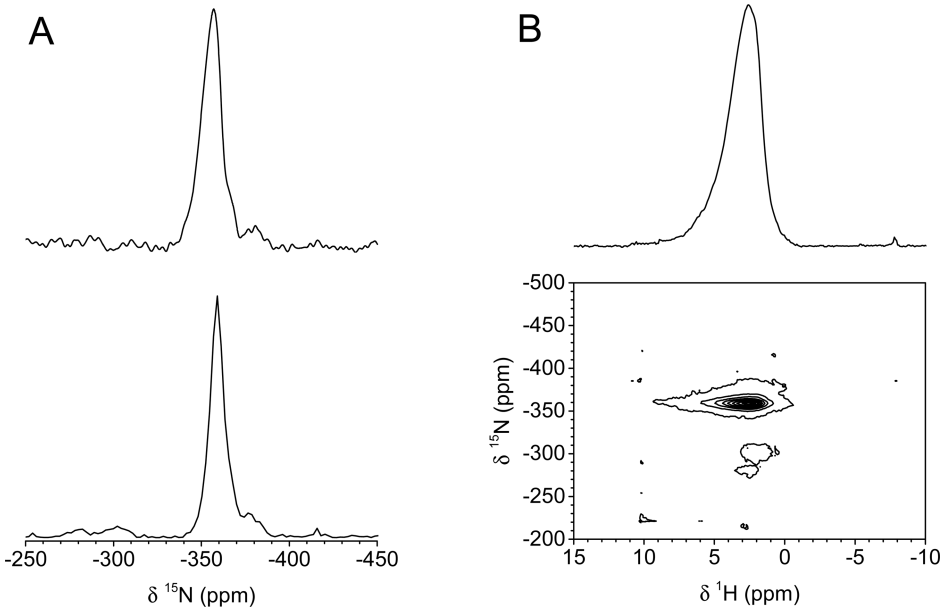


**Figure 4.** (A) Top spectrum: DNP-enhanced $^{15}$N CPMAS spectrum of $Zr(NMe_2)_n$@MSN under natural $^{15}$N abundance. The spectrum was obtained at ∼100 K using $\nu_R$ = 10 kHz; $\nu_{RF}(^{1}H)$ = 100 kHz, 107 kHz, and 100 kHz during hard pulse, cross-polarization, and SPINAL $^{1}$H decoupling; $\nu_{RF}(^{15}N)$ = ∼ 87 kHz during cross-polarization; $\tau_{CP}$ = 4 ms; 2048 scans; and $\tau_{RD}$ = 4 s. Lower spectrum: skyline $^{15}$N projection of the 2D $^{15}$N−$^{1}$H idHetcor spectrum in figure (B). (B) 2D $^{15}$N−$^{1}$H idHetcor spectrum of $^{15}$N-enriched $Zr(^{15}NMe_2)_n$@MSN. The spectrum was obtained at 14.1 T, using $\nu_R$ = 34 kHz; $\nu_{RF}(^{1}H)$ = 100 kHz during 90° pulse and 91 kHz during CP, and 10 kHz during SPINAL-64 $^{1}$H decoupling; $\nu_{RF}(^{15}N)$ = 62 kHz during 90° pulse and 57 kHz during CP, and 10 kHz during SPINAL-64 $^{15}$N decoupling; 128 rows with $\Delta t_1$ = 30 μs; 64 scans per row, and STATES-TPPI acquisition with $\tau_{RD}$ = 2 s.



DOI: 10.1021/acscatal.5b01671
ACS Catal. 2015, 5, 7399−7414

abundance in just over 2 h (Figure 4A, top spectrum). The spectrum features a single, fairly broad signal at −355 ppm, which we assign to Zr-bound $NMe_2$ groups. To further investigate their nature, a series of DNP-enhanced CPMAS $^{15}N$ NMR spectra were measured as a function of $\tau_{CP}$ contact time. The buildup of $^{1}H-^{15}N$ cross-polarization (Figure S5 in SI), which is governed by the heteronuclear dipolar coupling, and thus can be used to evaluate the $^{1}H-^{15}N$ distance,[56] indicates that the $^{15}N$ nuclei are polarized primarily by $^{1}H$ nuclei at a distance of about 2 Å, which is consistent with protons in $NMe_2$ groups being the source. Interestingly, the local maxima in the curve (which were reproducibly measured several times, and evaluated using eq 20c in ref 49), suggest that a small fraction of the $^{1}H-^{15}N$ pairs reside at a distance of ∼1.0 Å, as would be expected in zirconium amine species. This finding implies that the resonance centered at −355 ppm can be assigned to dimethylamide groups and a small amount of dimethylamine coordinated to surface-bonded zirconium sites.

We decided to verify that the surface Zr species observed by DNP did not result from the reaction with the solvent or the nitroxide radicals. To this end, we synthesized labeled $Zr(^{15}NMe_2)_4$ from isotopically enriched $Me_2{}^{15}NH{\cdot}HCl$ through the sequence shown in Scheme 1. The intermediate species

**Scheme 1. Synthesis of Labeled $Zr(^{15}NMe_2)_4$**

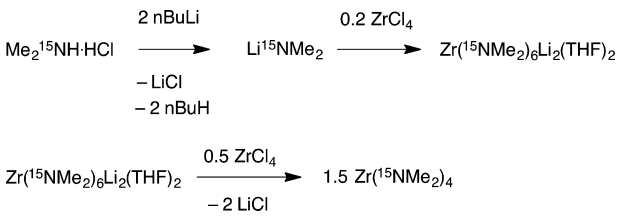


$Zr(NMe_2)_6Li_2THF_2$ was previously reported from the reaction of $Zr(NMe_2)_4$ and 2 equiv of $LiNMe_2$.[52] Here it is synthesized directly from $ZrCl_4$ and $LiNMe_2$, and we report its $^{15}N$ NMR chemical shift at −295 ppm.

The reaction of $Zr(^{15}NMe_2)_6Li_2THF_2$ and 0.5 equiv of $ZrCl_4$ gives pure $Zr(^{15}NMe_2)_4$ as its $^{15}N$ labeled isotopomer ($^{15}N$ NMR in benzene-$d_6$: −306 ppm). The grafting reaction was repeated with the labeled $Zr(^{15}NMe_2)_4$ sample to produce $Zr(^{15}NMe_2)_n$@MSN and $H^{15}NMe_2$ ($^{15}N$ NMR in benzene-$d_6$: −366 ppm). A 2D $^{15}N-^{1}H$ correlation spectrum of $Zr(^{15}NMe_2)_n$@MSN was acquired under fast (34 kHz) MAS using the indirect detection of $^{15}N$ nuclei for sensitivity enhancement ($^{15}N-^{1}H$ idHetcor, see Figure 4B).[57] In agreement with the DNP-based experiment, the idHetcor measurement showed a dominant correlation between the $^{1}H$ NMR signal at ∼2.4 ppm and $NMe_2$ groups resonating at around −355 ppm. A minor peak at −370 ppm most likely represents small concentration of free $HNMe_2$ left within the pores.

In addition, note that $Zr(NMe_2)_n$@MSN features close to 1 mmol of functional groups per 385 $m^2$ of surface, which corresponds to the coverage of ∼70%. Thus, the grafting reaction provides the maximum zirconium amide loading. We may further speculate that the distinction between ≡$SiOZr(NMe_2)_3$, $(\equiv SiO)_2Zr(NMe_2)_2(NHMe_2)$, and $(\equiv SiO)_2Zr(NMe_2)_2$ may relate to steric effects controlled by this surface coverage. The distinction between the surface species obtained in our grafting experiments versus the cyclometalated ≡$SiOZr(\eta^2\text{-}NMeCH_2)(NMe_2)(NHMe_2)$ may also relate to these intersite steric effects. In particular, $silica_{700}$, which is dehydroxylated at 700 °C under vacuum to give isolated silanols, reacts to provide only monopodal surface structures. In the 550 °C calcined MSN used in our study, a bipodal zirconium-surface interaction relieves the intersite steric pressure rather than $\beta$-abstraction that would give the zirconacyclopropane structure.

The $^{15}N$ NMR experiments also rule out the presence of ≡$SiNMe_2$ surface groups, which could form by addition of Zr−$NMe_2$ across a strained Si−O−Si surface site. This conclusion is based on the featureless region of the $^{15}N$ NMR experiments from −300 to −350 ppm. The $^{15}N$ NMR signal for ≡$SiNMe_2$ is expected to be ca. −330 ppm based on the $^{15}N$ NMR chemical shift of the model compound $(EtO)_3SiNMe_2$ ($^{15}N$ NMR, benzene-$d_6$: −326 ppm). A summary of all findings that support the composition of $Zr(NMe_2)_n$@MSN as a primarily ≡$SiOZr(NMe_2)_3$, with smaller amounts of $(\equiv SiO)_2Zr(NMe_2)_2$ and $(\equiv SiO)_2Zr(NMe_2)_2(NHMe_2)$ is given in Table 2.

**Synthesis and Characterization of ZrH/Bpin@MSN.** The reaction of $Zr(NMe_2)_n$@MSN and HBpin, which produces

**Table 2. Characterization Experiments and Conclusions Regarding the Nature of $Zr(NMe_2)_n$@MSN**

| experiment | observation | interpretation |
|---|---|---|
| electron microscopy/ EDX | well-dispersed Zr | no Zr or $ZrO_2$ clusters formed |
| reaction stoichiometry | 1.2 mmol $HNMe_2$ detected/g MSN | |
| | 1.0 mmol $Zr(NMe_2)_4$ consumed/g MSN | |
| ICP-OES | 0.91 mmol Zr/g | zirconium loading established |
| C, N combustion analysis | 4.9 mmol C/g, 2.5 mmol N/g | Zr:$NMe_2$ ∼ 1:2.7 suggests a 3:7 mixture of $Zr(NMe_2)_2$ and $Zr(NMe_2)_3$ groups |
| $^{13}C$ DPMAS/spin counting | 2.7 mmol $NMe_2$/g | Zr:$NMe_2$ ∼ 1:3 suggests primarily three $NMe_2$-containing ligands/ Zr |
| IR | new $\nu_{CH}$ bands at ∼2900 $cm^{-1}$ | $NMe_2$ groups present on surface |
| | $\nu_{OH}$ band at 3747 $cm^{-1}$ not detected | isolated silanols have reacted with $Zr(NMe_2)_4$ |
| $^{15}N$ SSNMR: | strong signal at −355 ppm polarized by Me groups, weakly by H | nitrogen is primarily present as dimethylamide groups |
| MSN + $HNMe_2$, $^{13}C$ NMR: | weak peak at 36 ppm | only a small amount of $HNMe_2$ physisorbs to calcined MSN |
| IR analysis: | $\nu_{OH}$ band at 3747 $cm^{-1}$ and weak intensity NH and CH bands are detected | |
| reaction with HBpin (below) | 2.5 mmol $Me_2NBpin$ formed/g $Zr(NMe_2)_n$@MSN | ca. 2.7 reactive $NMe_2$ groups per Zr center |



DOI: 10.1021/acscatal.5b01671
ACS Catal. 2015, 5, 7399−7414

the zirconium hydride surface species discussed below, also further characterizes the zirconium amide sites by quantification of reactive $NMe_2$ groups (eq 2). A micromolar-scale reaction of

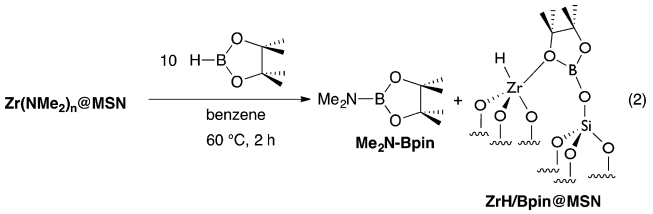


$Zr(NMe_2)_n$@MSN and excess HBpin affords 2.5 mmol of $Me_2NBpin$ per gram of material, which was quantified by integration of product signals with respect to a known concentration of $Si(SiMe_3)_4$ as an internal standard. In the $^1H$ NMR spectrum of the soluble portion of the reaction mixture, a resonance at 2.62 ppm was assigned to the $NMe_2$ moiety of $Me_2NBpin$. In the corresponding solution-phase $^{11}B$ NMR spectrum, a singlet at 24.2 ppm was assigned to $Me_2NBpin$,[58] and a doublet at 28.5 ppm ($^1J_{BH}$ = 174 Hz) represented unreacted HBpin. The reaction of $^{15}N$-labeled $Zr(^{15}NMe_2)_n$@MSN yields an isotopically enriched sample of $Me_2{}^{15}NBpin$. The $^{15}N$ NMR chemical shift of this material appears at −350 ppm, and this value will be used to assign surface species (see below). The amount of $Me_2NBpin$ quantified by integration suggests that approximately 2.8 $NMe_2$ groups are accessible per zirconium center, again indicating that the predominant surface species in $Zr(NMe_2)_n$@MSN contains three $NMe_2$ groups per zirconium. Finally, this experiment rules out the presence of any cyclometalated amide in this sample because the interaction of two equivalents of HBpin and the ≡SiOZr(NMeCH$_2$)(NMe$_2$)(NHMe$_2$) surface moiety would give pinB−NMeCH$_2$−Bpin, and that species was not detected in the solution-phase $^{11}B$ NMR spectrum.

The ZrH/Bpin@MSN sample was synthesized following the reaction given by eq 2. To facilitate the ensuing discussion of this product, whose identification proved to be very challenging, we first consider an independent reaction 3 of HBpin on calcined MSN. The ICP measurement of the resulting material, referred to as Bpin@MSN, indicates a boron loading of 1.33 mmol/g.

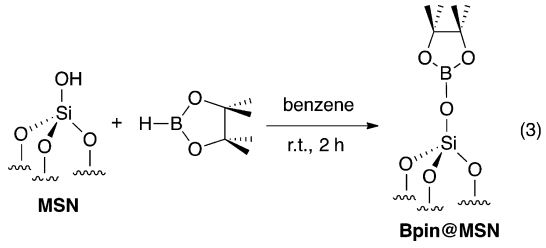


A $^{11}B$ DPMAS experiment on Bpin@MSN revealed a single resonance, which, based on the observed NMR shift ($\delta \approx 19$ ppm, see Figure 5A, dashed line), must be attributed to trigonally coordinated boron species. We note that the MAS NMR spectra of half-integer quadrupolar nuclei, such as $^{11}B$, are broadened by the quadrupolar interaction and that the NMR shifts ($\delta$) observed in such spectra consist of contributions from the dominant chemical shifts ($\delta_{CS}$) and the so-called quadrupole induced shifts. On the basis of the discussion below, we estimate the $\delta_{CS}$ value for the boron species in Bpin@MSN to be around 21 ppm, which is close to one measured in the solution NMR spectrum of $PhCH_2OBpin$ (23 ppm), suggesting that the ≡SiOBpin groups are indeed a product of the reaction of eq 3. This conclusion is supported by two additional findings. First, the $^1H$ DPMAS spectrum of Bpin@MSN (Figure S6B in SI) features a dominant resonance at 1 ppm, consistent with one observed in the solution $^1H$ NMR spectrum of $PhCH_2O$-Bpin for the pinacol moiety (1.04 ppm). Second, as in the case of $^{15}N$ CPMAS, by measuring the buildup of $^1H \rightarrow {}^{11}B$ CP signal as a function of $\tau_{CP}$, we estimated the $^1H - {}^{11}B$ internuclear distance in Bpin@MSN at ∼3.4 Å (Figure S7A in SI), in good agreement with the average distance between the $^{11}B$ and methyl protons in Bpin.[56]

We now return to ZrH/Bpin@MSN produced by the reaction given by eq 2. First, ICP-OES measurements show similar zirconium loading (0.89 mmol/g) and boron loading (0.86 mmol/g), and that the loading of Zr from $Zr(NMe_2)_n$@MSN is unaffected by the treatment with HBpin. The $^{11}B$ spin counting experiment yielded 0.9 (±0.1) mmol/g of boron in ZrH/Bpin@MSN, in excellent agreement with the ICP-OES analysis. In the $^{11}B$ DPMAS spectrum of this sample, a broad signal appeared whose NMR shift ($\delta \approx 18$ ppm) is similar but not identical with that of Bpin@MSN discussed above (compare solid and dashed lines in Figure 5A). The 2D MQMAS experiment on this sample (Figure 5B), which removes the anisotropic broadening due to the second-order quadrupolar interaction and allows for determination of the pure chemical shift ($\delta_{CS}$),[59,60] shows that the $^{11}B$ chemical shift for this boron site is the same as in Bpin@MSN ($\delta_{CS} \approx 21$ ppm). The so-called isotropic (vertical) dimension of this spectrum revealed a small shoulder representing an additional resonance with $\delta_{CS} \approx 23$ ppm (vide infra), which most likely represents residual $Me_2NBpin$ trapped within the MSN pores.

We also measured the $^1H$ DPMAS and 2D $^1H-{}^{11}B$ Hetcor spectra of ZrH/Bpin@MSN (Figure 5C,D). Note that the $^1H$ projection of the Hetcor spectrum is very similar to the $^1H$ DPMAS spectrum. The dominant $^1H$ peak at ∼1 ppm is easily assigned to the protons of the methyl groups of Bpin, whereas one at ∼2.4 ppm corresponds to $^1H$ of a small amount of $Me_2N$ moiety. These results imply that ≡SiOBpin is the dominant boron-containing structure found in ZrH/Bpin@MSN. However, in addition to small difference in the observed shifts (Figure 5A), the chemical environments of this moiety in Bpin@MSN and in ZrH/Bpin@MSN samples are not identical. Indeed, the $^1H \rightarrow {}^{11}B$ CP dynamics indicated that the nearest $^1H-{}^{11}B$ internuclear distance is considerably shorter (∼2.1 Å, Figure S7B in SI) in the zirconium-containing sample. Note that these experiments do not establish the identity of the polarizing spin.

The $^{11}B$ NMR signals for $Me_2NBpin$ and ZrH/Bpin@MSN are unresolved under MAS alone and thus cannot be discerned in the Hetcor spectrum. Most likely, the correlation between the $^{11}B$ NMR signal and $^1H$ NMR signal at 2.4 ppm is assigned to the intermolecular interaction between the $^{11}B$ of abundant ≡Si−O−Bpin and $^1H$ of $Me_2NBpin$, as well as intramolecular interactions within $Me_2NBpin$ or ZrH/Bpin@MSN species.

Although we propose the surface organometallic species to be a zirconium hydride (eq 3), $^1H$ NMR resonances at >10 ppm that were previously assigned as $(≡SiO)_3ZrH$ and $(≡SiO)_2ZrH_2$[41] were notably absent from the $^1H$ NMR spectrum of the product from ≡SiOZr$(NMe_2)_3$ and HBpin. Despite the absence of those downfield $^1H$ resonances, a zirconium hydride species, albeit with a modified coordination sphere from (≡


DOI: 10.1021/acscatal.5b01671
ACS Catal. 2015, 5, 7399−7414

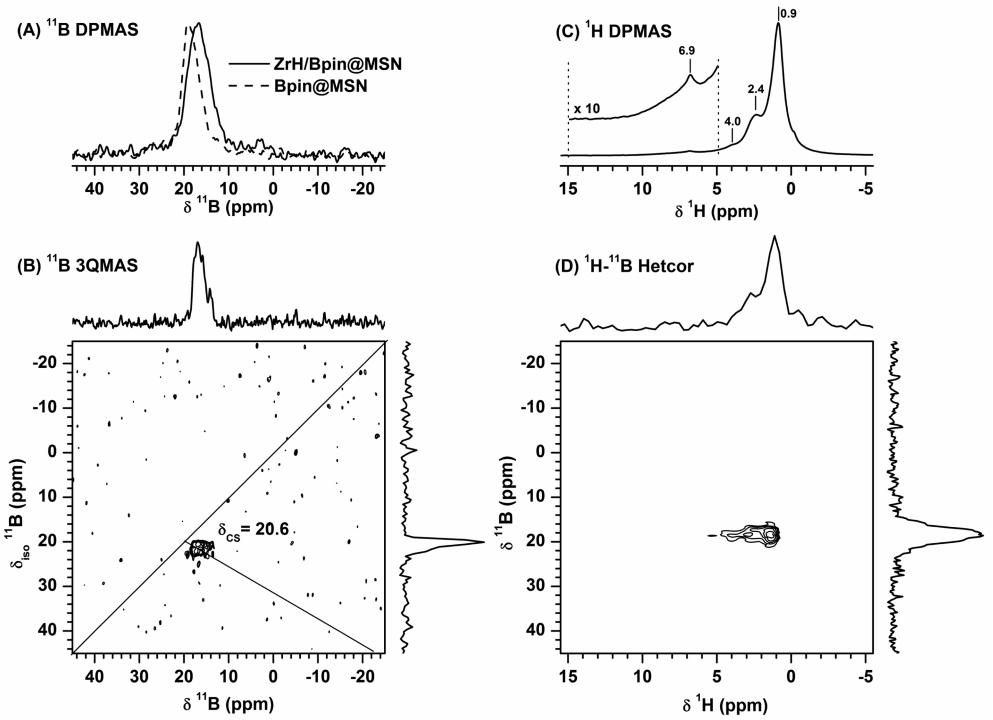


**Figure 5.** (A) $^{11}$B DPMAS spectra of Bpin@MSN (dashed line) and ZrH/Bpin@MSN (solid line), (B) 2D $^{11}$B 3QMAS spectrum of ZrH/Bpin@MSN, (C) $^{1}$H DPMAS spectrum of ZrH/Bpin@MSN, and (D) 2D $^{1}$H−$^{11}$B Hetcor spectrum of ZrH/Bpin@MSN. The spectra were obtained using $\nu_R$ = 25 kHz, with (A) $\nu_{RF}(^{11}B)$ = 125 kHz during hard pulse (corresponding to ∼10° flip angle), $\nu_{RF}(^{1}H)$ = 100 kHz during TPPM $^{1}$H decoupling, 8000 scans, and $\tau_{RD}$ = 1 s; (B) $\nu_{RF}(^{11}B)$ = 125 kHz and 15 kHz during hard and soft (z-filter) pulses, respectively, $\nu_{RF}(^{1}H)$ = 100 kHz during TPPM $^{1}$H decoupling, 64 rows with $\Delta t_1$ = 10 $\mu$s, 72 scans per row, and $\tau_{RD}$ = 1.5 s; (C) $\nu_{RF}(^{1}H)$ = 100 kHz during hard pulse, 4 scans, and $\tau_{RD}$ = 1 s; and (D) $\nu_{RF}(^{1}H)$ = 125 kHz, 75 kHz, and 100 kHz during 90° pulse, CP, and TPPM $^{1}$H decoupling, $\nu_{RF}(^{11}B)$ = 50 kHz during CP, $\tau_{CP}$ = 2 ms, 64 rows with $\Delta t_1$ = 20 $\mu$s, 96 scans per row, and $\tau_{RD}$ = 1 s.

$SiO)_3ZrH$ and $(\equiv SiO)_2ZrH_2$, is a proposed product of the reaction of $Zr(NMe_2)_n$@MSN and HBpin. In fact, the room-temperature, solution−solid interfacial reaction conditions of the hydroboration are mild with respect to the gas−solid 150 °C reaction of $\equiv SiOZr(CH_2CMe_3)_3$ that gives $(\equiv SiO)_3ZrH$ and $(\equiv SiO)_2ZrH_2$. That is, HBpin as a hydride source may provide access to new zirconium-hydride surface structures. Unfortunately, we are unaware of any reliable chemical shift information on structures such as $\equiv SiOZrH_3$; however, on the basis of the chemical shift trend for $(\equiv SiO)_3ZrH$ and $(\equiv SiO)_2ZrH_2$, the $^{1}$H NMR signal for $\equiv SiOZrH_3$ might be expected to be at least >12 ppm. In contrast to that trend, a small resonance at around 6.9 ppm is present in our sample (Figure 5C inset). This signal is not observed in the sample from the reaction of MSN and HBpin (Figure S6b in SI). The zirconium-bound hydrogen chemical shifts in $Cp^*_2ZrH_2$, $(Cp^*_2ZrH)_2O$, and $Cp^*_2ZrH(NH_2)$ ($Cp^* = C_5Me_5$) were reported to be 7.46, 5.5, and 4.82 ppm, respectively,[61,62] and even further upfield ZrH resonances were reported for $Cp^*_2ZrH(NH_2BH_3)$.[63] That is, association of pinacolborane or borate groups or amide moieties with a surface-bonded zirconium hydride might result in upfield chemical shifts with respect to $(\equiv SiO)_3ZrH$ and $(\equiv SiO)_2ZrH_2$. To test for the presence of a surface-supported zirconium hydride that is distinct from $(\equiv SiO)_3ZrH$ and $(\equiv SiO)_2ZrH_2$ and assign the $^{1}$H NMR signal at 6.9 ppm, the HBpin-treated solid was allowed to react with $D_2$ gas in benzene (eq 4).

Upon treatment with 1 atm of $D_2$, the signal at 6.9 ppm diminished 50%, and after 3 cycles with 1 atm of $D_2$, the signal

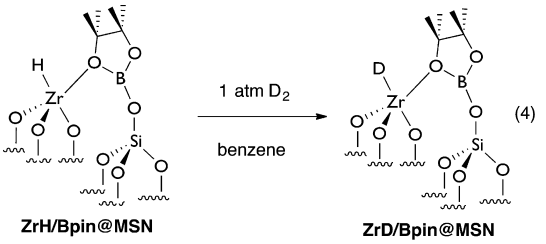


(4)

disappeared entirely (Figure 6). Interestingly, the $^{2}$H NMR spectrum from the reaction of ZrH/Bpin@MSN and $D_2$ gives only a signal at ∼2.5 ppm (Figure S8), suggesting that deuterium is incorporated in methyl groups. Unfortunately, a signal at ∼7 ppm could not be unambiguously identified above the noise. However, $^{2}$H DPMAS spectrum of ZrD/Bpin@MSN from the reaction of DBpin and $Zr(NMe_2)_n$@MSN contains signals at 7.3, 4.0, 2.5 (as a shoulder), and 1.5 ppm corresponding to deuterium incorporation into ZrH, $NMe_2$, and Bpin groups (Figure S9). On the basis of these facile H/D exchange reactions, this resonance is assigned as a zirconium hydride. Spin counting experiments indicate that the ZrH loading is ca. 0.5 mmol per gram, and thus surface ZrH sites account for >50% of the zirconium in the sample.

The infrared spectrum of the ZrH/Bpin@MSN solid product further supported this assignment (Figure 7B) on the basis of a band centered at 1592 $cm^{-1}$ that we assigned to a $\nu_{ZrH}$. The IR spectrum of MSN treated with HBpin does not contain signals in this region (Figure 7A). Previously, a signal at 1638 $cm^{-1}$ was assigned to the $\nu_{ZrH}$ in $(\equiv SiO)_3ZrH$.[41] Importantly, the



DOI: 10.1021/acscatal.5b01671
ACS Catal. 2015, 5, 7399−7414

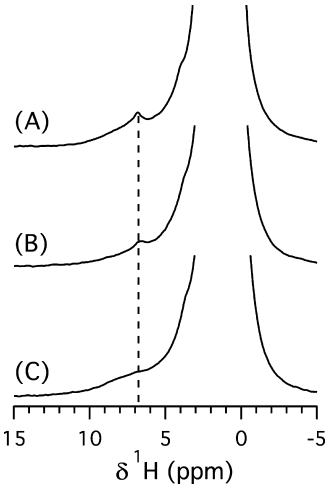


**Figure 6.** $^1$H DPMAS spectra of Zr(NMe$_2$)$_n$@MSN + 10 HBpin, (**A**) as synthesized, (**B**) 1× of $D_2$ exchange, (**C**) 3× of $D_2$ exchange. The spectra are normalized to the sample amount and show the absolute intensities. The spectra were obtained using $\nu_R$ = 40 kHz, $\nu_{RF}(^1H)$ = 125 kHz, and $\tau_{RD}$ = 20 s.

1592 cm$^{-1}$ peak was not detected in the IR spectrum of the ZrH/Bpin@MSN exposed to $D_2$, and this change is taken as evidence for the formation of ZrD/Bpin@MSN (Figure 7C). Unfortunately, the expected location of a $\nu_{ZrD}$ at 1125 cm$^{-1}$ overlaps with the silica absorptions, and that signal could not be detected. However, the signal at 1592 cm$^{-1}$ reappears upon addition of $H_2$ to ZrD/Bpin@MSN (Figure 7D). Interestingly, new broad signals at ∼2395 cm$^{-1}$ appear in the sample treated with $D_2$. Similar bands were observed in the spectrum resulting from treatment of Zr(NMe$_2$)$_n$@MSN with DBpin (Figure 7E); in that IR spectrum, the signal at 1592 cm$^{-1}$ was also not detected. These lower energy bands at ∼2395 cm$^{-1}$ may be attributed to H/D exchange reactions catalyzed by a surface zirconium hydride and correspond to signals of deuterium-exchanged pinacol and amido methyls. These observations are consistent with the $^1$H SSNMR results and support the characterization of this material as containing a zirconium hydride, including the expected H/D exchange reactivity.[6]

Finally, additional experiments were performed to account for the small amount of NMe$_2$ groups in the reaction of HBpin and Zr(NMe$_2$)$_n$@MSN (which produced only 2.5 mmol of Me$_2$NBpin vs 2.7 mmol per gram of Zr(NMe$_2$)$_n$@MSN). Combustion analysis of ZrH/Bpin@MSN revealed 0.4 ± 0.05 mmol of nitrogen per gram of material. This value is significantly reduced in comparison to the Zr(NMe$_2$)$_n$@MSN starting sample. Therefore, a $^{15}$N−$^{15}$H idHetcor experiment was used to probe the identity of the nitrogen species (Figure 8). There is a correlation from a $^{15}$N NMR signal at −355 ppm

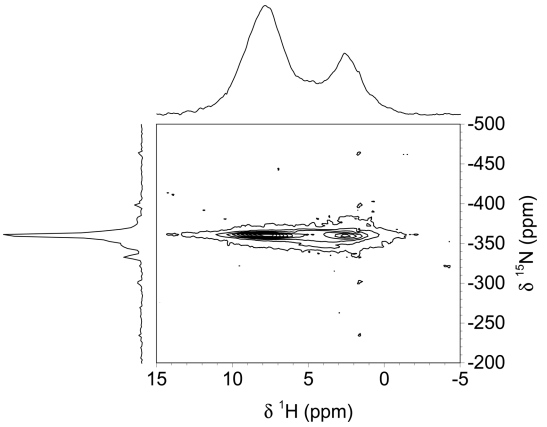


**Figure 8.** 2D $^{15}$N−$^1$H idHetcor spectrum of $^{15}$N-enriched ZrH/Bpin@MSN. The spectrum was obtained at 14.1 T, using $\nu_R$ = 34 kHz; $\nu_{RF}(^1H)$ = 100 kHz during 90° pulse and 91 kHz during CP, and 10 kHz during SPINAL-64 $^1$H decoupling; $\nu_{RF}(^{15}N)$ = 62 kHz during 90° pulse and 57 kHz during CP pulse, and 10 kHz during SPINAL-64 $^{15}$N decoupling; 128 rows with $\Delta t_1$ = 30 μs; 64 scans per row, and STATES-TPPI acquisition with $\tau_{RD}$ = 2 s.

to a $^1$H NMR resonance at 2.4 ppm. On the basis of the similarity of this chemical shift to Me$_2$NBpin and the $^{11}$B NMR signal at 24 ppm, we attribute the residual $^{15}$N SSNMR signal

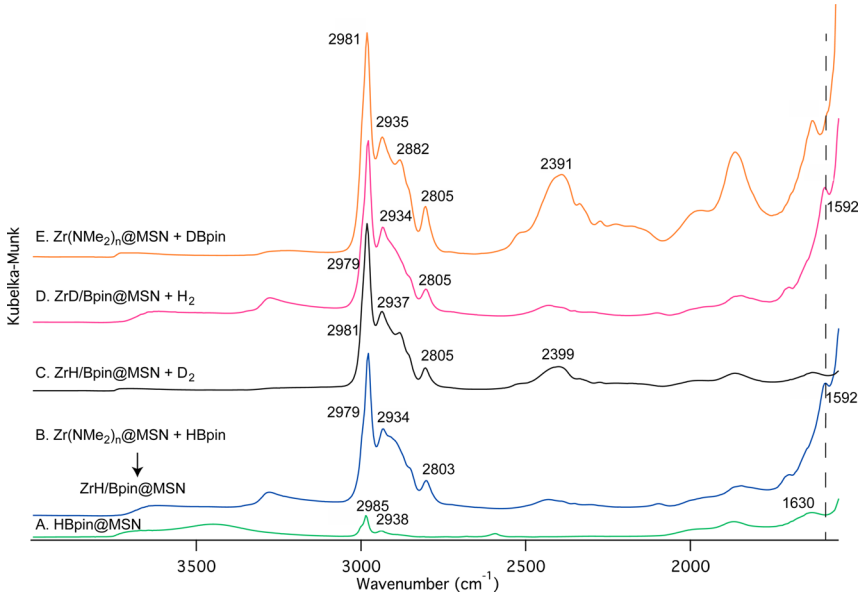


**Figure 7.** Diffuse reflectance IR spectra of (A) Bpin@MSN, (B) ZrH/Bpin@MSN, (C) ZrH/Bpin@MSN + $D_2$, (D) ZrD/Bpin@MSN + $H_2$, and (E) Zr(NMe$_2$)$_n$@MSN + DBpin.



DOI: 10.1021/acscatal.5b01671
*ACS Catal.* 2015, 5, 7399−7414

Table 3. Characterization Experiments and Conclusions Regarding the Nature of ZrH/Bpin@MSN

| experiments | observations | interpretations |
|---|---|---|
| reaction stoichiometry: $Zr(NMe_2)_n$@MSN + HBpin | 2.5 mmol $Me_2NBpin$ formed/g $Zr(NMe_2)_n$@MSN | all but ca. 0.2 mmol $NMe_2$/g are desorbed from the material |
| reaction side products: | | |
| $Zr(NMe_2)_n$@MSN + HBpin | small amount of $H_2$ formed | few reactive silanols or NH groups present in $Zr(NMe_2)_n$@MSN |
| MSN + HBpin | large amount of $H_2$ formed | |
| ICP-OES: | | the Zr:B ratio is ∼ 1:1. |
| $Zr(NMe_2)_n$@MSN + HBpin: | 0.89 mmol Zr/g material<br>0.86 mmol B/g material | HBpin treatment does not leach Zr from MSN |
| MSN + HBpin: | 1.33 mmol B/g material | Bpin is grafted to the material |
| IR | $\nu_{ZrH}$ observed at 1592 $cm^{-1}$ | zirconium hydride formed using HBpin that is distinct from $(\equiv SiO)_3ZrH$ |
| reaction with $D_2$, then $H_2$ | band at 1592 $cm^{-1}$ disappears upon $D_2$ addition, then reappears upon $H_2$ addition | exchangable zirconium hydride |
| $^1H$ SSNMR: | $\delta_{ZrH}$ at 6.9 ppm, 0.5 mmol H/g | the zirconium hydride surface species is distinct from $(\equiv SiO)_3ZrH$ |
| treatment with $D_2$ | signal disappears upon $D_2$ addition | |
| $^{11}B$ SSNMR: | | the $\equiv$SiOBpin chemical environment is influenced by surface Zr species |
| MSN + HBpin | $\delta \approx 19$ ppm; $\delta_{CS} \approx 21$ ppm; $^1H-^{11}B$ distance ∼3.4 Å | |
| $Zr(NMe_2)_n$@MSN + HBpin | $\delta \approx 18$ ppm; $\delta_{CS} \approx 21$ ppm; $^1H-^{11}B$ distance ∼2.1 Å | |
| $^{11}B$ NMR spin count | 0.9 mmol B/g | |
| $^1H-^{15}N$ Hetcor | −355 ppm $^{15}N$ signal correlates with 7.9 ppm $^1H$ signal | residual $NMe_2$ groups unreactive due to zirconium-coordination and H-bonding |

partly to surface-absorbed $Me_2NBpin$. Furthermore, there is also a correlation between the $^{15}N$ SSNMR signal at −355 ppm and a signal in the $^1H$ NMR dimension at 7.9 ppm. These chemical shifts, as well as the $^1H-^{15}N$ correlation, suggest that some of the remaining surface nitrogen is present as $Zr-NHMe_2$.

The evidence supporting the identity of ZrH/Bpin@MSN as a zirconium hydride formed from reaction of $Zr(NMe_2)_n$@MSN and HBpin is given in Table 3, and a description of the spectroscopy and structural assignment is summarized in the conclusion.

**Catalytic Hydroboration of Carbonyls.** On the basis of the facile reaction of $Zr(NMe_2)_n$@MSN and HBpin, this material was investigated as a catalyst for the hydroboration of carbonyl compounds with pinacolborane. Initially, benzaldehyde was used as a test substrate to compare the reactivity of supported zirconium with possible background reactions and homogeneous analogues. With grafted amidozirconium as the precatalyst (5 mol %, based on ICP-OES-determined zirconium loading), quantitative conversion of benzaldehyde to its pinacolborane ester is accomplished at room temperature after 2 h in benzene-$d_6$, as determined by $^1H$ NMR spectroscopy (eq 5). Control experiments, in which PhCHO

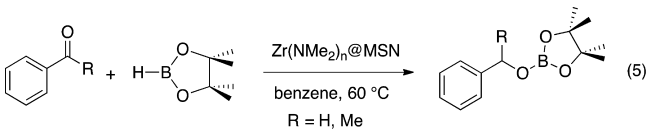

(5)

and HBpin are mixed in benzene at room temperature with or without MSN, give only trace quantities of product (Table 4). In addition, the minimal conversion of PhCHO and HBpin occur to the same extent with the zirconium-free material Bpin@MSN, obtained from the reaction of MSN and HBpin, as the slow, uncatalyzed background reaction. Thus, the zirconium sites present in the $Zr(NMe_2)_n$@MSN material are responsible for catalytic activity.

Further support for this idea is provided by related homogeneous catalysis. The compound $Zr(NMe_2)_4$ is an effective catalyst for this carbonyl hydroboration reaction, as is $\{PhB(Ox^{Me2})_2C_5H_4\}Zr(NMe_2)_2$.[46] In the presence of 5 mol % of either soluble complex, quantitative conversion of PhCHO to $PhCH_2OBpin$ is observed after 30 min in benzene-$d_6$ at 60 °C. The faster conversion obtained with homogeneous versus heterogeneous catalysts may result from the effect of diffusion, a lower percentage of active sites or slower site activation in the supported catalyst, or simply the effect of silica as a ligand for zirconium in this catalysis.

The hydroboration using $Zr(NMe_2)_n$@MSN as the catalyst is selective in the presence of a number of functional groups, as determined by conversion of substituted benzaldehydes shown in Table 5. Aldehyde substrates containing ethers (*p*-methoxybenzaldehyde and furfural), nitro groups (*p*-nitrobenzaldehyde), halides (*p*-chlorobenzaldehyde), alkyl substitution (*p*-tolualdehyde), an aliphatic aldehyde (cyclohexanecarboxaldehyde), and ferrocene substitution (ferrocene-2-carboxaldehyde) are readily reduced, although *para*-chlorobenzaldehyde required 5× greater reaction time than benzaldehyde. *Para*-substitution by formyl or pinacolborane ester groups does not impact the reacting moiety as assessed by the hydroboration of *p*-phthaldialdehyde which gives 1,4-bis(pinacolborane ester)-benzene. Equivalent amounts of the solvent, reactants, and catalysts are used in each experiment for consistency and straightforward comparisons between substrates.

The hydroboration of ketones is also efficiently catalyzed by $Zr(NMe_2)_n$@MSN. A background screen of catalyst-free conditions, calcined MSN, or Bpin@MSN as catalysts for the addition of acetophenone and pinacolborane only returned unreacted acetophenone, even with heating to 100 °C (see Table 6). A loading of 5 mol % $Zr(NMe_2)_n$@MSN catalyzes quantitative formation of 1-phenylethoxyborane ester after 24 h at room temperature in benzene. However, 60 °C appears to be a generally appropriate temperature for convenient rates of conversion. As in the aldehyde hydroboration examples,


DOI: 10.1021/acscatal.5b01671
ACS Catal. 2015, 5, 7399−7414

Table 4. Catalytic Hydroboration of Benzaldehyde and Acetophenone with Pinacolborane[a]

| Reaction | Catalyst (5 mol %) | Temp. (°C) | Time (h) | Conv. (%)[b] |
|---|---|---|---|---|
| 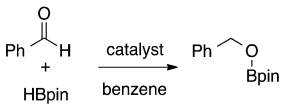 | No cat | 25 | 1 | Trace |
| | MSN | 25 | 1 | 0 |
| | $Zr(NMe_2)_4$ | 25 | 0.5 | >99 |
| | $Zr(NMe_2)_n$@MSN | 25 | 2 | >99 |
| | $\{PhB(Ox^{Me2})_2C_5H_4\}Zr(NMe_2)_2$ | 25 | 0.5 | >99 |
| 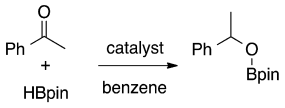 | No cat | 25-100 | 2 | 0 |
| | MSN | 25-100 | 2 | 0 |
| | $Zr(NMe_2)_4$ | 25 | 1 | >99 |
| | $Zr(NMe_2)_4$ | 60 | 0.5 | >99 |
| | $Zr(NMe_2)_n$@MSN | 25 | 24 | >99 |
| | $Zr(NMe_2)_n$@MSN | 60 | 2 | >99 |
| | $\{PhB(Ox^{Me2})_2C_5H_4\}Zr(NMe_2)_2$ | 25 | 10 | >99 |
| | $\{PhB(Ox^{Me2})_2C_5H_4\}Zr(NMe_2)_2$ | 60 | 1 | >99 |

[a]5 mol % catalyst in benzene-$d_6$ using 1.3 equiv of HBpin. [b]Obtained by integration of product signal in comparison to $Si(SiMe_3)_4$ as an internal standard.

reactions of acetophenone and HBpin with 5 mol % $Zr(NMe_2)_4$ or $\{PhB(Ox^{Me2})_2C_5H_4\}Zr(NMe_2)_2$ (under homogeneous conditions) is accomplished in shorter times than with 5 mol % $Zr(NMe_2)_n$@MSN.

As in the aldehyde hydroboration, aliphatic substituents with $\alpha$-hydrogen are reduced without production of pinacolborane enolate ester side products that might form through substrate deprotonation (Table 6). Linear aliphatic ketones are reduced more rapidly than cyclic aliphatic or aryl-substituted ketones. Ketones containing nitroarene or trifluoromethyl groups are readily reduced without affecting the functionality. In addition, $\alpha,\beta$-unsaturated ketones are reduced selectively at the carbonyl, leaving the carbon−carbon double-bond intact. Benzophenone and fluorenone are also reduced in good yield, with fluorenone showing faster conversion under equivalent conditions.

A possible intermediate in the zirconium-catalyzed carbonyl hydroboration is a zirconium alkoxy moiety of the type [Zr]−OCHRR′. The reaction of such an intermediate with pinacolborane to form a B−O bond is not necessarily straightforward given the oxophilicity of zirconium. We should note, however, that our recently proposed boron-centered zwitterionic mechanism for a magnesium-catalyzed hydroboration of esters avoids the magnesium alkoxide intermediate.[24] A related mechanism could bypass the Zr−O bond in the current catalysis. Despite this possibility, magnesium alkoxides and HBpin react to give pinacolborane esters. Moreover, the surface-supported zirconium amide and HBpin react to give $Me_2NBpin$.

Thus, the intermediacy of [Zr]OCHRR′ is not ruled out, and there are (at least) two types of Zr−O bonds present in a possible $(\equiv SiO)_nX_{3-n}Zr-OCHRR'$ intermediate, a siloxide-zirconium bond and an alkoxide-zirconium bond. Both moieties might be capable of reaction with HBpin, with the reaction of ≡SiOZr bonds potentially resulting in catalyst leaching. In order to test for this possibility, the $Zr(NMe_2)_n$@MSN was reacted with excess HBpin and the MSN product was analyzed. Low-angle powder XRD (Figure S1 in SI) and TEM measurements (Figure 1D,E) indicated that the pore structure and particle morphology were not affected by the pinacolborane. In addition, EDX measurements (Figure 1F) show that the well-distributed zirconium remains unchanged after treatment with HBpin. Thus, the zirconium-surface interaction and the silica wall structure is maintained in the presence of HBpin.

A number of additional experiments also were performed to test for zirconium leaching. First, the catalytic material was isolated by filtration, washed with benzene, dried under vacuum, and reused in hydroboration of benzaldehyde or acetophenone. This sequence was performed eight times with both PhCHO and PhC(O)Me as substrates without apparent loss of catalytic activity (Figure 9). The reactions were monitored during the conversion, verifying that ∼2 h are required for full conversion in the first and eighth cycles. Moreover, plots of acetophenone concentration versus time roughly follow exponential decay, with the observed pseudo first-order rate constants after 1, 4, and 8 recycles being $4 \times 10^{-4}$ $s^{-1}$, $4 \times 10^{-4}$ $s^{-1}$, and $3 \times 10^{-4}$ $s^{-1}$. Thus, the rates of catalysis are not significantly diminished with repeated catalyst recycling. In the first cycle with $Zr(NMe_2)_n$@MSN as the precatalyst, the $Me_2NBpin$ byproduct of catalyst activation is present in the crude RR′HCO−Bpin product. This substance was not observed during subsequent cycles, and pure boronate ester product is obtained after filtration and evaporation of volatile materials.

Second, the zirconium loading on MSN after catalysis, as determined by ICP-OES, is identical within error to the loadings after grafting of $Zr(NMe_2)_4$ on calcined MSN and after heating at 60 °C in benzene. The same weight % Zr is obtained for the ZrH/Bpin@MSN material, as obtained from



DOI: 10.1021/acscatal.5b01671
ACS Catal. 2015, 5, 7399−7414

Table 5. $Zr(NMe_2)_n$@MSN-Catalyzed Hydroboration of Aldehydes with Pinacolborane[a]

| Catalytic Conversion | Time (h) | Conv. (%)[b] | Boronate Yield (%)[c] | Alcohol Yield (%)[d] |
|---|---|---|---|---|
| 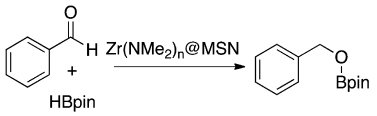 | 2 | >99 | 98 | 95 |
| 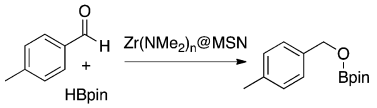 | 2 | >99 | 97 | 95 |
| 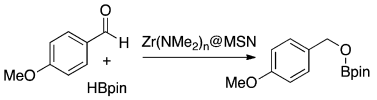 | 2 | >99 | 98 | 95 |
| 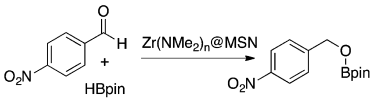 | 2 | >99 | 98 | 96 |
| 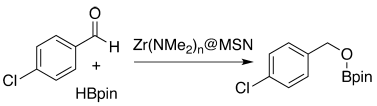 | 10 | >99 | 97 | 95 |
| 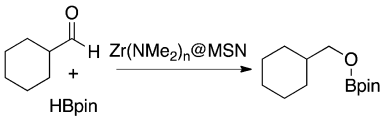 | 3 | >99 | 98 | 94 |
| 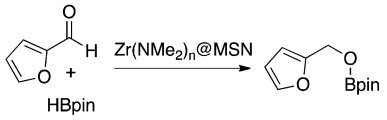 | 3 | >99 | 98 | 95 |
| 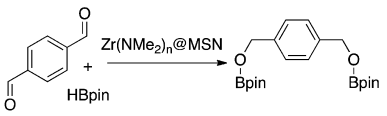 | 2 | >99[e] | 98 | 95 |
| 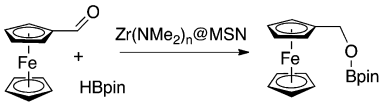 | 3 | >99 | 98 | n.a. |

[a]All the reactions are carried with 5 mol % $Zr(NMe_2)_n$@MSN in benzene-$d_6$ at room temperature using 1.3 equiv of HBpin. [b]Obtained by integration of $RCH_2OBpin$ signal against $Si(SiMe_3)_4$ as an internal standard. [c]Isolated yields for $RCH_2OBpin$ product. [d]Isolated yield of $RCH_2OH$ product after hydrolysis with NaOH. [e]2 equiv of HBpin was used.

the reaction of HBpin and $Zr(NMe_2)_n$@MSN and after catalytic hydroboration reactions (Table 1). In addition, a catalytic reaction mixture was filtered after 50% conversion to give a mixture of PhCOMe, HBpin, and PhMeHCO-Bpin, and the soluble portion of the reaction mixture was heated at 60 °C. The ratio of starting material and product in this separated solution-phase portion is invariant over 1 h (i.e., no further conversion), whereas full conversion to PhMeHCO−Bpin is observed in an unfiltered parallel experiment. Finally, the supernatant was evaporated after a catalytic reaction, and only a trace amount of zirconium (0.001 mM) was detected by ICP-OES. These experiments reinforce the robust nature of the supported zirconium catalyst and the supported nature of the hydroboration catalyst.

## CONCLUSION

The reaction of $Zr(NMe_2)_4$ and calcined mesoporous silica provides $Zr(NMe_2)_n$@MSN, a material containing zirconium sites with a Zr:$NMe_2$ ratio of ∼1:2.7. Detailed SSNMR studies, particularly indirectly detected $^{15}N$ Hetcor experiments and DNP-enhanced CPMAS $^{15}N$ NMR spectra, reveal that zirconium is primarily bonded to dimethylamide groups, with a small amount of coordinated dimethylamine. These data, together with quantitative $^{13}C$ SSNMR and elemental analysis, characterize the surface zirconium species as containing three



DOI: 10.1021/acscatal.5b01671
ACS Catal. 2015, 5, 7399−7414

Table 6. $Zr(NMe_2)_n$@MSN-Catalyzed Hydroboration of Ketones with Pinacolborane[a]

| Reaction | Time (h) | Conv. (%)[b] | Boronate Yield (%)[c] | Alcohol Yield (%)[d] |
|---|---|---|---|---|
| 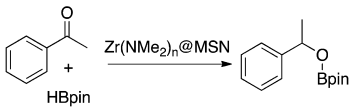 | 2 | >99 | 97 | 91 |
| 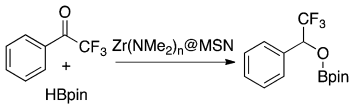 | 2 | >99 | 97 | 92 |
| 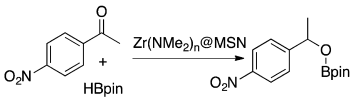 | 2 | >99 | 95 | 92 |
| 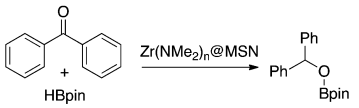 | 4 | >99 | 97 | 94 |
|  | 2 | >99 | 98 | 93 |
| 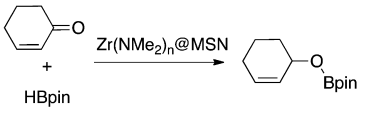 | 1 | >99 | 98 | 92 |
| 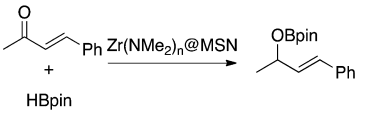 | 3 | >99 | 95 | 90 |
| 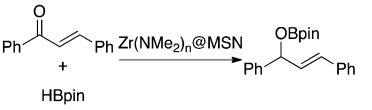 | 7 | >99 | 96 | 91 |
| 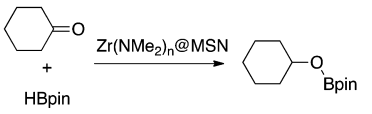 | 1 | >99 | 98 | 92 |
| 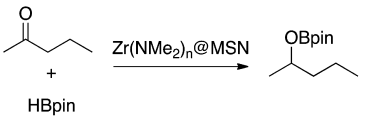 | 0.5 | >99 | 91 | 87 |
| 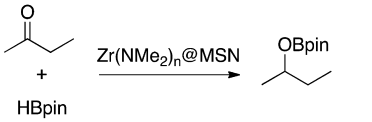 | 0.5 | >99 | 90 | 85 |

[a]All the reactions are carried with 5 mol % catalyst in benzene-$d_6$ at 60 °C using 1.3 equiv of HBpin. [b]Obtained by integration of $R_2CHOBpin$ signal against $Si(SiMe_3)_4$ as an internal standard. [c]Isolated yields for $R_2CHOBpin$. [d]Isolated yield for $R_2CHOH$.

sites: primarily (more than 70%) coordinated by three nitrogen-containing ligands, with the remaining sites (up to 30%) as the dipodal $(\equiv SiO)_2Zr(NMe_2)_2$. Moreover, the former sites are a mixture of mainly monopodal $\equiv SiOZr(NMe_2)_3$ (more than 90%) with the small remaining amount as diamido amine $(\equiv SiO)_2Zr(NMe_2)_2(NHMe_2)$. The basis for



DOI: 10.1021/acscatal.5b01671
ACS Catal. 2015, 5, 7399−7414

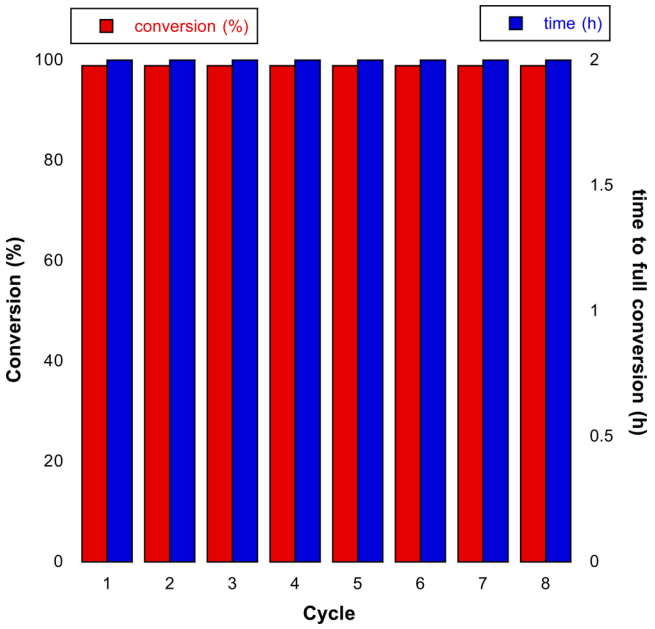


**Figure 9.** Catalyst recycling experiments. Quantitative conversion and >99% selectivity for acetophenone hydroboration is observed after reisolation and reapplication of the catalyst for at least eight cycles. In situ monitoring of the catalytic reactions indicated that ∼2 h is required for full conversion in each recycle experiment.

this conclusion is the reactivity of $Zr(NMe_2)_n$@MSN with HBpin. Around 85−90% of the surface $NMe_2$ groups react with HBpin to give $Me_2NBpin$, and the remaining nitrogen groups are likely present as either zirconium-coordinated and hydrogen-bond species or physisorbed $Me_2NBpin$. This assignment is supported by the characteristic $^{15}N$ SSNMR chemical shift (−355 ppm), the nitrogen correlation with a broad downfield hydrogen signal in $^{15}N-^{1}H$ Hetcor experiments, and the high reactivity of both dimethylamine and dimethyl amidozirconium groups toward pinacolborane. The latter observations suggest that the unreactive $NMe_2$ are in chemically distinct environments from free $HNMe_2$ and $ZrNMe_2$ moieties, and coordination to zirconium and the involvement of the $NMe_2$ groups in hydrogen-bonding to the silica surface may explain their inert nature.

The surface species formed in the reaction of $Zr(NMe_2)_n$@MSN and HBpin, namely, ZrH/Bpin@MSN, was characterized by $^{1}H$ and $^{11}B$ SSNMR and infrared spectroscopies. In this MSN system, the reaction of HBpin and silanol groups provides ≡SiOBpin, and the interaction of these groups and surface zirconium species perturbs the chemical environment of the surface Bpin groups. $^{1}H$ NMR and infrared spectroscopies reveal signals assigned to zirconium hydride, and these assignments are supported by selective H/D exchange reactions of zirconium hydride and $D_2$ or zirconium deuteride with $H_2$. Thus, the reaction of HBpin and $Zr(NMe_2)_n$@MSN provides a zirconium hydride that shows the anticipated reactivity of such a species in H/D exchange reactions.

The present work has demonstrated that surface-supported, catalytically active zirconium hydrides are accessible from amides and likely from metal alkoxides or hydroxides using HBpin as the hydride source. That notion is advanced by characterization data and the catalytic hydroboration studies, which may involve the zirconium hydride and zirconium alkoxides as catalytic intermediates. The zirconium sites on MSN are active in carbonyl hydroboration even after exposure of the catalytic materials to air. For example, reaction of $Zr(NMe_2)_n$@MSN and air produces detectable amounts of $HNMe_2$, but the addition reaction of HBpin and acetophenone is readily catalyzed by the hydrolyzed material under the conditions of Table 4. Thus, this MSN-supported early transition metal system is a capable, robust catalyst for the reduction of oxygenated organic compounds.

Although the catalytic reduction of oxygenates by early transition metal sites has previously been demonstrated with homogeneous catalysis, zirconium hydrides are typically associated with extreme sensitivity to air and moisture. This list of highly sensitive species includes silica surface-supported zirconium hydrides, which have previously shown high reactivity toward inert substrates such as methane.[1,3,6,40] Although the apparent rate of hydroboration with surface-supported $Zr(NMe_2)_n$@MSN is lower than the homogeneous zirconium catalysts, the accessibility of a catalytically active species even after air exposure and the recyclability of the surface-supported catalyst provide appealing advantages for the heterogeneous system. We are currently exploring other hydride sources to access surface-supported hydrides for new catalytic applications.

## ■ ASSOCIATED CONTENT

### Supporting Information

The Supporting Information is available free of charge on the ACS Publications website at DOI: 10.1021/acscatal.5b01671.

Powder XRD patterns, $^{1}H$ NMR spectra of $Zr(NMe_2)_4$ grafting and HBpin reactions for quantification, and catalysis products, and solid-state $^{1}H$ and $^{11}B$ DPMAS NMR spectra (PDF)

## ■ AUTHOR INFORMATION


### Corresponding Authors

*E-mail: sadow@iastate.edu.

*E-mail: mpruski@iastate.edu.

### Present Address

‡Exxon-Mobil


### Notes

The authors declare no competing financial interest.

## ■ ACKNOWLEDGMENTS

This research was supported by the U.S. Department of Energy, Office of Basic Energy Sciences, Division of Chemical Sciences, Geosciences, and Biosciences through the Ames Laboratory (Contract No. DE-AC02-07CH11358). The authors thank BASF for the generous donation of the P104 surfactant.

## ■ REFERENCES


(1) Quignard, F.; Choplin, A.; Basset, J.-M. *J. Chem. Soc., Chem. Commun.* **1991**, 1589−1590.

(2) Zakharov, V. A.; Dudchenko, V. K.; Paukshtis, E. A.; Karakchiev, L. G.; Yermakov, Y. I. *J. Mol. Catal.* **1977**, *2*, 421−435.

(3) Thieuleux, C.; Quadrelli, E. A.; Basset, J.-M.; Dobler, J.; Sauer, J. *Chem. Commun.* **2004**, 1729−1731.

(4) Zakharov, V. A.; Yermakov, Y. I. *Catal. Rev.: Sci. Eng.* **1979**, *19*, 67−103.

(5) Yermakovt, Y. I.; Ryndin, Y. A.; Alekseev, O. S.; Kochubey, D. I.; Shmachkov, V. A.; Gergert, N. I. *J. Mol. Catal.* **1989**, *49*, 121−132.

(6) Casty, G. L.; Matturro, M. G.; Myers, G. R.; Reynolds, R. P.; Hall, R. B. *Organometallics* **2001**, *20*, 2246−2249.




DOI: 10.1021/acscatal.5b01671
*ACS Catal.* 2015, 5, 7399−7414

(7) Basset, J.-M.; Coperet, C.; Soulivong, D.; Taoufik, M.; Cazat, J. T. *Acc. Chem. Res.* **2009**, *43*, 323−334.
(8) Copéret, C.; Chabanas, M.; Petroff Saint-Arroman, R.; Basset, J.-M. *Angew. Chem., Int. Ed.* **2003**, *42*, 156−181.
(9) Lécuyer, C.; Quignard, F.; Choplin, A.; Olivier, D.; Basset, J.-M. *Angew. Chem., Int. Ed. Engl.* **1991**, *30*, 1660−1661.
(10) Quignard, F.; Lécuyer, C.; Choplin, A.; Olivier, D.; Basset, J.-M. *J. Mol. Catal.* **1992**, *74*, 353−363.
(11) Carter, M. B.; Schiott, B.; Gutierrez, A.; Buchwald, S. L. *J. Am. Chem. Soc.* **1994**, *116*, 11667−11670.
(12) Fu, P.-F.; Brard, L.; Li, Y.; Marks, T. J. *J. Am. Chem. Soc.* **1995**, *117*, 7157−7168.
(13) Gountchev, T. I.; Tilley, T. D. *Organometallics* **1999**, *18*, 5661−5667.
(14) Molander, G. A.; Julius, M. *J. Org. Chem.* **1992**, *57*, 6347−6351.
(15) Molander, G. A.; Retsch, W. H. *Organometallics* **1995**, *14*, 4570−4575.
(16) Takahashi, T.; Hasegawa, M.; Suzuki, N.; Saburi, M.; Rousset, C. J.; Fanwick, P. E.; Negishi, E. *J. Am. Chem. Soc.* **1991**, *113*, 8564−8566.
(17) Xin, S. X.; Harrod, J. F. *Can. J. Chem.* **1995**, *73*, 999−1002.
(18) Jeske, G.; Lauke, H.; Mauermann, H.; Schumann, H.; Marks, T. J. *J. Am. Chem. Soc.* **1985**, *107*, 8111−8118.
(19) Tilley, T. D. *Acc. Chem. Res.* **1993**, *26*, 22−29.
(20) Gauvin, F.; Harrod, J. F.; Woo, H. G. *Adv. Organomet. Chem.* **1998**, *42*, 363−405.
(21) Waterman, R. *Organometallics* **2013**, *32*, 7249−7263.
(22) Arrowsmith, M.; Hadlington, T. J.; Hill, M. S.; Kociok-Kohn, G. *Chem. Commun.* **2012**, *48*, 4567−4569.
(23) Harrison, K. N.; Marks, T. J. *J. Am. Chem. Soc.* **1992**, *114*, 9220−9221.
(24) Mukherjee, D.; Ellern, A.; Sadow, A. D. *Chem. Sci.* **2014**, *5*, 959−964.
(25) Arrowsmith, M.; Hill, M. S.; Hadlington, T.; Kociok-Kohn, G.; Weetman, C. *Organometallics* **2011**, *30*, 5556−5559.
(26) Anker, M. D.; Arrowsmith, M.; Bellham, P.; Hill, M. S.; Kociok-Kohn, G.; Liptrot, D. J.; Mahon, M. F.; Weetman, C. *Chem. Sci.* **2014**, *5*, 2826−2830.
(27) Oluyadi, A. A.; Ma, S.; Muhoro, C. N. *Organometallics* **2012**, *32*, 70−78.
(28) Khalimon, A. Y.; Farha, P.; Kuzmina, L. G.; Nikonov, G. I. *Chem. Commun.* **2012**, *48*, 455−457.
(29) Koren-Selfridge, L.; Query, I. P.; Hanson, J. A.; Isley, N. A.; Guzei, I. A.; Clark, T. B. *Organometallics* **2010**, *29*, 3896−3900.
(30) Evans, D. A.; Fu, G. C. *J. Org. Chem.* **1990**, *55*, 5678−5680.
(31) Hadlington, T. J.; Hermann, M.; Frenking, G.; Jones, C. *J. Am. Chem. Soc.* **2014**, *136*, 3028−3031.
(32) Verdaguer, X.; Lange, U. E. W.; Reding, M. T.; Buchwald, S. L. *J. Am. Chem. Soc.* **1996**, *118*, 6784−6785.
(33) Willoughby, C. A.; Buchwald, S. L. *J. Am. Chem. Soc.* **1994**, *116*, 11703−11714.
(34) Willoughby, C. A.; Buchwald, S. L. *J. Am. Chem. Soc.* **1994**, *116*, 8952−8965.
(35) Yun, J.; Buchwald, S. L. *J. Am. Chem. Soc.* **1999**, *121*, 5640−5644.
(36) Pereira, S.; Srebnik, M. *Organometallics* **1995**, *14*, 3127−3128.
(37) Eter, M. E.; Hamzaoui, B.; Abou-Hamad, E.; Pelletier, J. D. A.; Basset, J.-M. *Chem. Commun.* **2013**, *49*, 4616−4618.
(38) Beaudoin, M.; Scott, S. L. *Organometallics* **2000**, *20*, 237−239.
(39) Hamzaoui, B.; Eter, M. E.; Abou-hamad, E.; Chen, Y.; Pelletier, J. D. A.; Basset, J.-M. *Chem. - Eur. J.* **2015**, *21*, 4294−4299.
(40) Pasha, F. A.; Bendjeriou-Sedjerari, A.; Huang, K.-W.; Basset, J.-M. *Organometallics* **2014**, *33*, 3320−3327.
(41) Rataboul, F.; Baudouin, A.; Thieuleux, C.; Veyre, L.; Coperet, C.; Thivolle-Cazat, J.; Basset, J. M.; Lesage, A.; Emsley, L. *J. Am. Chem. Soc.* **2004**, *126*, 12541−12550.
(42) Brown, H. C. *Hydroboration*; W. A. Benjamin: New York, 1962.
(43) Gaylord, N. G. *Reduction with Complex Metal Hydrides*; Interscience: New York, 1956.
(44) Kandel, K.; Frederickson, C.; Smith, E. A.; Lee, Y.-J.; Slowing, I. I. *ACS Catal.* **2013**, *3*, 2750−2758.
(45) Diamond, G. M.; Jordan, R. F.; Petersen, J. L. *J. Am. Chem. Soc.* **1996**, *118*, 8024−8033.
(46) Manna, K.; Ellern, A.; Sadow, A. D. *Chem. Commun.* **2010**, *46*, 339−341.
(47) Gutekunst, G.; Brook, A. G. *J. Organomet. Chem.* **1982**, *225*, 1−3.
(48) Gilman, H.; Smith, C. L. *J. Organomet. Chem.* **1967**, *8*, 245−253.
(49) Wu, J. Y.; Moreau, B.; Ritter, T. *J. Am. Chem. Soc.* **2009**, *131*, 12915−12917.
(50) Lesage, A.; Lelli, M.; Gajan, D.; Caporini, M. A.; Vitzthum, V.; Miéville, P.; Alauzun, J.; Roussey, A.; Thieuleux, C.; Mehdi, A.; Bodenhausen, G.; Coperet, C.; Emsley, L. *J. Am. Chem. Soc.* **2010**, *132*, 15459−15461.
(51) Zagdoun, A.; Casano, G.; Ouari, O.; Schwarzwälder, M.; Rossini, A. J.; Aussenac, F.; Yulikov, M.; Jeschke, G.; Copéret, C.; Lesage, A.; Tordo, P.; Emsley, L. *J. Am. Chem. Soc.* **2013**, *135*, 12790−12797.
(52) Chisholm, M. H.; Hammond, C. E.; Huffman, J. C. *Polyhedron* **1988**, *7*, 2515−2520.
(53) Fujdala, K. L.; Tilley, T. D. *J. Am. Chem. Soc.* **2001**, *123*, 10133−10134.
(54) Quignard, F.; Lecuyer, C.; Bougault, C.; Lefebvre, F.; Choplin, A.; Olivier, D.; Basset, J. M. *Inorg. Chem.* **1992**, *31*, 928−930.
(55) Troullier, N.; Martins, J. L. *Phys. Rev. B: Condens. Matter Mater. Phys.* **1991**, *43*, 1993−2006.
(56) Amoureux, J. P.; Pruski, M. *Mol. Phys.* **2002**, *100*, 1595−1613.
(57) Althaus, S. M.; Mao, K.; Stringer, J. A.; Kobayashi, T.; Pruski, M. *Solid State Nucl. Magn. Reson.* **2014**, *57*−*58*, 17−21.
(58) Solé, C.; Fernández, E. *Angew. Chem., Int. Ed.* **2013**, *52*, 11351−11355.
(59) Medek, A.; Harwood, J. S.; Frydman, L. *J. Am. Chem. Soc.* **1995**, *117*, 12779−12787.
(60) Fernandez, C.; Pruski, M. *Solid State NMR*; Chan, J. C. C., Ed.; Springer: Berlin, 2012; Vol. *306*, pp 119−188.
(61) Manriquez, J. M.; McAlister, D. R.; Sanner, R. D.; Bercaw, J. E. *J. Am. Chem. Soc.* **1976**, *98*, 6733−6735.
(62) Hillhouse, G. L.; Bercaw, J. E. *J. Am. Chem. Soc.* **1984**, *106*, 5472−5478.
(63) Almqvist, F.; Torstensson, L.; Gudmundsson, A.; Frejd, T. *Angew. Chem., Int. Ed. Engl.* **1997**, *36*, 376−377.


DOI: 10.1021/acscatal.5b01671
*ACS Catal.* 2015, 5, 7399−7414